Analysis of glycosylinositol phosphorylceramides expressed by the opportunistic mycopathogen *Aspergillus fumigatus*

Marcos S. Toledo,[*] Steven B. Levery,[1,†] Beau Bennion,[†] Luciana L. Guimaraes,[*] Sherry A. Castle,[†] Rebecca Lindsey,[§] Michelle Momany,[§] Chaeho Park,[**] Anita H. Straus,[*] and Helio K. Takahashi[1,*]

Department of Biochemistry,* Universidade Federal de São Paulo/Escola Paulista de Medicina, 04023-900 São Paulo, Brazil Department of Chemistry,† University of New Hampshire, Durham, NH 03824-3598; Department of Plant Biology,§ University of Georgia, Athens, GA 30602-7271; and Department of Biochemistry and Molecular Biology,** University of Georgia, Athens, GA 30602-7229

Abstract **Acidic glycosphingolipid components were extracted from the opportunistic mycopathogen *Aspergillus fumigatus* and identified as inositol phosphorylceramide and glycosylinositol phosphorylceramides (GIPCs). Using nuclear magnetic resonance sppectroscopy, mass spectrometry, and other techniques, the structures of six major components were elucidated as Ins-P-Cer (Af-0), Man*p*(α1→3)Man*p*(α1→2)Ins-P-Cer (Af-2), Man*p*(α1→2)Man*p*(α1→3)Man*p*(α1→2)Ins-P-Cer (Af-3a), Man*p*(α1→3)[Gal*f*(β1→6)]Man*p*(α1→2)-Ins-P-Cer (Af-3b), Man*p*(α1→2)-Man*p*(α1→3)[Gal*f*(β1→6)]Man*p*(α1→2)Ins-P-Cer (Af-4), and Man*p*(α1→3)Man*p*(α1→6)Glc*p*N(α1→2)Ins-P-Cer (Af-3c) (where Ins = *myo*-inositol and *P* = phosphodiester). A minor *A. fumigatus* GIPC was also identified as the *N*-acetylated version of Af-3c (Af-3c*), which suggests that formation of the GlcNα1→2Ins linkage may proceed by a two-step process, similar to the GlcNα1→6Ins linkage in glycosylphosphatidylinositol (GPI) anchors (transfer of GlcNAc, followed by enzymatic de-*N*-acetylation). The glycosylinositol of Af-3b, which bears a distinctive branching Gal*f*(β1→6) residue, is identical to that of a GIPC isolated previously from the dimorphic mycopathogen *Paracoccidioides brasiliensis* (designated Pb-3), but components Af-3a and Af-4 have novel structures. Overlay immunostaining of *A. fumigatus* GIPCs separated on thin-layer chromatograms was used to assess their reactivity against sera from a patient with aspergillosis and against a murine monoclonal antibody (MEST-1) shown previously to react with the Gal*f*(β1→6) residue in Pb-3.** These results are discussed in relation to pathogenicity and potential approaches to the immunodiagnosis of *A. fumigatus*.—Toledo, M. S., S. B. Levery, B. Bennion, L. L. Guimaraes, S. A. Castle, R. Lindsey, M. Momany, C. Park, A. H. Straus, and H. K. Takahashi. **Analysis of glycosylinositol phosphorylceramides expressed by the opportunistic mycopathogen *Aspergillus fumigatus*. *J. Lipid Res.* 2007.** 48: **1801–1824.**

Supplementary key words fungus • sphingolipid • glycolipid • galactofuranose • monoclonal antibody • electrospray ionization • ion trap • mass spectrometry • NMR spectroscopy

Of >185 fungal species to which humans are exposed, aspergilli are perhaps the most common; conidia (spores) from a variety of *Aspergillus* species, such as *A. versicolor*, *A. niger*, *A. terreus*, *A. flavus*, and *A. fumigatus*, can be found at high concentrations in both rural and urban environments, outdoors as well as within human habitations (1). Of these species, *A. fumigatus* is considered the most pathogenic and is now recognized as the most prevalent airborne fungal pathogen in developed countries (2, 3), even in hospital environments, where it may contribute only a small fraction of the aerial spore count (4). Along with the general increase in the number of immunocompromised patients as a result of the use of corticoids (5), organ transplants, human immunodeficiency virus infection, and cancer (6), the high thermotolerance of *A. fumigatus*, which is able to grow in temperatures varying from <20°C to at least 50°C, as well as its high sporulating capacity and the small size of its spores (2–3 μm) (1), have contributed to the prevalence of *A. fumigatus* in invasive and noninvasive human aspergillosis worldwide.

Abbreviations: 1-D and 2-D, one-dimensional and two-dimensional; CID, collision-induced decomposition; COSY, correlation spectroscopy; D_2O, deuterium oxide; ESI, electrospray ionization; GIPC, glycosylinositol phosphorylceramide; GPI, glycosylphosphatidylinositol; HPTLC, high-performance thin-layer chromatography; HSQC, heteronuclear single-quantum correlation; Ins, *myo*-inositol; IPC, inositol phosphorylceramide; MALDI-TOF, matrix-assisted laser desorption time-of-flight; R_f, retention factor; TOCSY, total correlation spectroscopy.

[1] To whom correspondence should be addressed.
e-mail: slevery@cisunix.unh.edu (S.B.L.); takahashi.bioq@epm.br (H.K.T.)

The online version of this article (available at http://www.jlr.org) contains additional two figures and one scheme.

Manuscript received 28 March 2007.
Published, JLR Papers in Press, May 8, 2007.
DOI 10.1194/jlr.M700149-JLR200

Currently, the most commonly used drugs for the treatment of aspergillosis are amphotericin B, which binds membrane sterol and creates transmembrane channels leading to an increase in membrane permeability to monovalent cations (7), and itraconazole, which competes for oxygen at the catalytic heme site of cytochrome P450/lanosterol 14α-demethylase, leading to an inhibition of ergosterol biosynthesis and the accumulation of 14α-methylated sterols in the fungal plasma membrane (8). However, these two drugs have major disadvantages, including the nephrotoxicity of amphotericin B and the lack of itraconazole preparations for intravenous application, limiting its use in patients with impaired bowel absorption. In addition, there are increasing reports documenting the development of resistance to these antifungal drugs among a variety of species, including *Aspergillus* (8). Thus, there exists a compelling interest in the discovery of new targets for the development of antifungal therapeutics: novel functional molecules and the pathways by which they are generated and interact with other components in processes essential for fungal reproduction and growth or host colonization.

Studies carried out during the 1990s demonstrated that many species of fungi are vulnerable to inhibitors of sphingolipid biosynthesis (reviewed in Ref. 9). This has stimulated increased interest in the structure, biosynthesis, and functional roles of fungal sphingolipids as potential targets for antifungal agents. A particularly interesting target is the fungal inositol phosphorylceramide (IPC) synthase (10), inhibitors of which are highly toxic to many mycopathogens but exhibit low toxicity in mammals (11–13). IPC synthase, generally believed to be encoded by orthologous *AUR1/IPC1* genes discovered in *Saccharomyces cerevisiae*, *Schizosaccharomyces pombe*, *Candida* species, *Aspergillus* species, and *Cryptococcus neoformans* (10, 14–18), catalyzes the transfer of *myo*-inositol-1-phosphate from phosphatidylinositol to ceramide. Neither IPC, IPC synthase, nor any orthologous *AUR1/IPC1* genes have been found in mammals, consistent with the lack of susceptibility of mammalian species to inhibitors of this enzyme.

Further processing of IPC by glycosyltransferases yields glycosylinositol phosphorylceramides (GIPCs), a class of complex anionic glycosphingolipids widely distributed among fungal species (19). Isolation and detailed characterization of GIPCs from a variety of fungi has begun to reveal an extensive structural diversity (see Discussion), the expression of which is considerably dependent on species and, apparently, at least in some mycopathogens, strongly regulated during morphogenesis (20–24). A total of ~30 distinct GIPC structures have been identified to date, with the discovery rate increasing during the last 5–6 years, based on further elaboration of three well-confirmed core structures distinguishable at the monoglycosyl level (**Scheme 1**).

Antigenic glycoside determinants are expressed on some fungal GIPC components, suggesting their potential as targets for immunodiagnostic reagents and the possibility of therapy based on stimulation of the mammalian humoral response (20, 21, 25–29). Elucidation of such immunological interactions calls for further detailed knowledge of the structures of these compounds, which is still limited compared with what is known about glycosphingolipids of animal species.

Here, we report on the structure elucidation of GIPCs from *A. fumigatus*. Among other observations, these studies revealed the presence of GIPCs containing an antigenic branched ±R→Man*p*(α1→3)[Gal*f*(β1→6)]Man*p*(α1→2)Ins structural motif. Although one GIPC antigen isolated from *A. fumigatus*, Man*p*(α1→3)[Gal*f*(β1→6)]Man*p*(α1→2)InsPCer (**Af-3b**), was characterized previously as a major GIPC component of the dimorphic mycopathogen *Paracoccidioides brasiliensis* (30), other GIPCs characterized here, including structural isomers and derivatives of **Af-3b**, have not been identified previously. A third major triglycosyl-IPC component of *A. fumigatus* was characterized as Man*p*(α1→3)Man*p*(α1→6)Glc*p*N(α1→2)Ins1-P-1Cer (**Af-3c**); in addition, a minor component with an *N*-acetylated GlcN residue was identified (**Af-3c***). Although the de-*N*-acetylated Glc*p*N(α1→2)Ins1-P-1-Cer core has been reported in GIPCs of several fungi (23, 31), this is the first time a GIPC containing a Glc*pNAc*(α1→2)Ins1-P-1Cer core, a presumptive intermediate in this biosynthetic pathway, has been identified.

EXPERIMENTAL PROCEDURES

Fungal isolates and growth conditions

A. fumigatus American Type Culture Collection strain 9197 was used for most preparations. Also used was *A. fumigatus* strain 237, originally cultured from open lung biopsy from a patient with invasive aspergillosis at Hope Hospital in Manchester, UK (a gift of Dr. David Holden, Hammersmith Hospital, London, UK). Approximately 5×10^9 spores were inoculated to 200 ml or 1 liter of complete medium (1% glucose, 0.2% peptone, 0.1% yeast extract, 0.1% casamino acids, nitrate salts, trace elements, and 0.01% vitamins, pH 6.5; trace elements, vitamins, nitrate salts, and amino acid supplements are described in the appendix to Ref. 32), incubated at 30°C or 37°C with shaking (200 rpm) for 24 h, filtered, and processed as described. Yields were 6–8 g wet weight per 200 ml of medium or 25–35 g wet weight per 1 liter of medium.

Solvents for extraction and anion-exchange chromatography

Solvent A consisted of isopropanol-hexane-water (55:20:25, v/v/v; upper phase discarded). Solvent B consisted of chloroform-methanol (2:1, v/v). Solvent C consisted of chloroform-methanol-water (30:60:8, v/v/v).

High-performance thin-layer chromatography

Analytical high-performance thin-layer chromatography (HPTLC) was performed on silica gel 60 plates (E. Merck, Darmstadt, Germany) using chloroform-methanol-water [50:47:14 (v/v/v), containing 0.038% (w/v) $CaCl_2$; solvent D] as the mobile phase. Lipid samples were dissolved in solvent B and applied by streaking from 5 μl Micro-caps (Drummond, Broomall, PA). Detection was with Bial's orcinol reagent [0.55% (w/v) orcinol and 5.5% (v/v) H_2SO_4 in ethanol-water (9:1, v/v); the plate is sprayed and heated briefly to ~200–250°C].

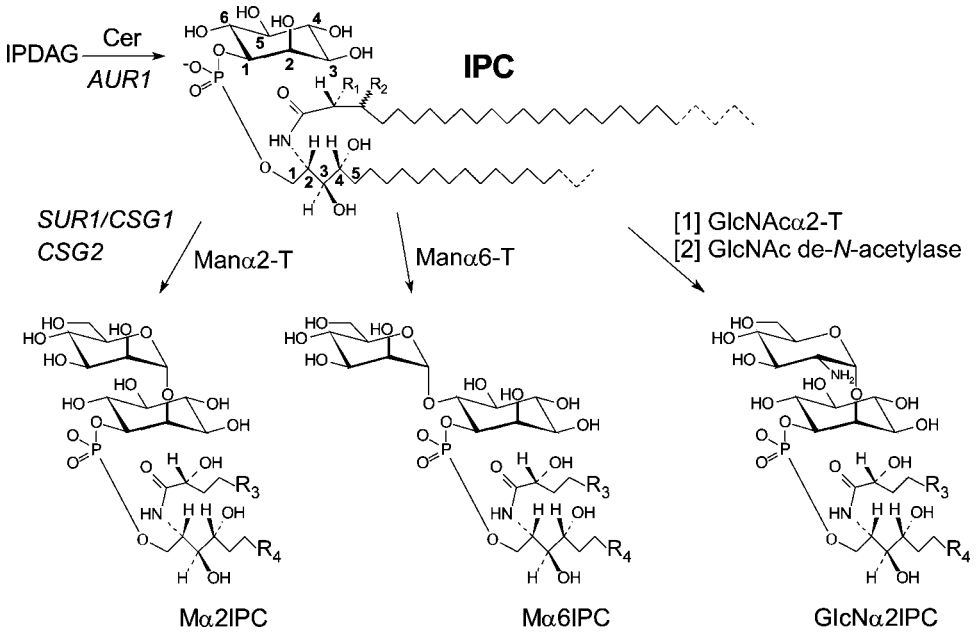

Scheme 1. Biosynthesis of fungal GIPCs, starting with transfer of *myo*-inositol-1-O-phosphate (IP) from diacylglycerol (DAG) moiety of phosphatidylinositol to ceramide, catalyzed by *AUR1* gene encoded IPC synthase. The observation of three intermediate core structures diverging at the monosaccharide level implies the existence of at least three distinct glycosyltransferases capable of using IPC as the acceptor: (i) Manα2-T (function requires two genes in *Saccharomyces cerevisiae*, *SUR1/CSG1* and *CSG2*), making Manα1→2InsPCer (Mα2IPC); (ii) Manα6-T, making Manα1→6InsPCer (Mα6IPC); (iii) GlcNAcα2-T, followed by action of de-*N*-acetylase, making GlcNα1→2InsPCer (GlcNα2IPC).

HPTLC immunostaining

Immunostaining of purified fungal GIPCs separated by HPTLC was performed by the procedure of Magnani, Smith, and Ginsburg (33), as modified by Kannagi et al. (34), with some additional changes to the HPTLC protocol. Briefly, separation by HPTLC was carried out in three steps. After application of GIPCs, the HPTLC plates were developed twice with chloroform-methanol (4:1, v/v; solvent E) and once with chloroform-methanol-water [30:18:4 (v/v/v), containing 0.020% (w/v) $CaCl_2$; solvent F). After HPTLC development, plates were dried, soaked in 0.5% polymethacrylate in hexane, dried again, and blocked for 2 h with 1% BSA in 0.01 M PBS, pH 7.2. Plates were then incubated with monoclonal antibody MEST-1 or aspergillosis serum overnight; this was followed by sequential incubation with either rabbit anti-mouse IgG or rabbit anti-human IgG, respectively, and ^{125}I-labeled protein A (4×10^5 cpm/ml) (35).

Extraction and purification of glycosphingolipids

Extraction and purification of glycosphingolipids were carried out as described previously (27, 36, 37), but with some modifications and additional steps introduced for the purpose of reducing the amounts of irrelevant substances to be dealt with earlier in the protocol. Briefly, glycosphingolipids were extracted by homogenizing mycelia (25–35 g wet weight) in an Omni-mixer (Sorvall, Inc., Wilmington, DE) three times with 200 ml of solvent A and three times with 200 ml of solvent B. The six extracts were pooled, dried on a rotary evaporator, dialyzed against water, and lyophilized. The dried residue was partitioned between water and 1-butanol presaturated with water (200 ml each) with vigorous shaking in a separatory funnel. The lower (water) layer was removed and similarly extracted three more times with equal volumes of water-saturated 1-butanol. The four 1-butanol extracts were combined in a round-bottom flask, evaporated to dryness, resuspended in a minimal volume of solvent C, and applied to a column of DEAE-Sephadex A-25 (Ac^- form). Neutral glycosphingolipids were eluted with 5 volumes of solvent C. Acidic glycosphingolipids were eluted with 5 volumes of 0.5 M sodium acetate in methanol. The acidic fraction was dried, dialyzed exhaustively against deionized water, redried, and treated with 20 ml of methanol-water-1-butanol (4:3:1, v/v/v) containing 25–30% methylamine at 55°C for 4 h (flask tightly stoppered), with occasional agitation. After removal of the reagent solution by rotary evaporation, the acidic lipids were further fractionated by repetitive preparative-scale HPLC, using columns of either 60 cm × 4.6 mm Iatrobeads (Iatron Chemical Co., Tokyo, Japan) 6RS-8010 or 50 cm × 4.6 mm Sphereclone (Phenomenex, Torrance, CA) 10 μm porous spherical silica. The mobile phase was a 2-propanol-hexane-water gradient programmed from 55:40:5 to 55:25:20 over 120 min, followed by isocratic elution for 40 min, with a flow rate of 0.5 ml/min. Generally, 40 × 2 ml fractions were collected for first-stage purifications and 80 × 1 ml fractions were collected for second-stage purifications, where required. The identity and purity of each fraction were assessed by analytical HPTLC as described above, and by one-dimensional (1-D) ^{1}H-NMR spectroscopy, before further characterization by the full range of NMR and MS techniques described below.

1-D ^{1}H- and 2-D ^{1}H-^{1}H and ^{1}H-^{13}C-nuclear magnetic resonance spectroscopy

Samples of underivatized (G)IPCs (~0.5–1.0 mg) were deuterium-exchanged by repeated lyophilization from deuterium oxide (D_2O) and then dissolved in 0.5 ml of DMSO-d_6/2% D_2O (30, 38) for NMR analysis. 1-D ^{1}H-NMR, 2-D ^{1}H-^{1}H- gradient enhanced correlation spectroscopy (gCOSY), ^{1}H-^{1}H total correlation spectroscopy (TOCSY), and proton-detected ^{1}H-^{13}C- gradient en-

hanced heteronuclear single-quantum correlation (gHSQC) experiments were performed at 35°C on Varian (Palo Alto, CA) Unity Inova 500 MHz (Department of Chemistry, University of New Hampshire) and 600 and 800 MHz (Complex Carbohydrate Research Center, University of Georgia) spectrometers using standard acquisition software available in the Varian VNMR software package. Proton chemical shifts are referenced to internal tetramethylsilane ($\delta = 0.000$ ppm). Carbon chemical shifts are referenced to solvent DMSO ($\delta = 40.0$ ppm); in some cases, these were not obtained from directly detected 1-D spectra but measured in F1 of the gHSQC experiment; therefore, the values are given to single decimal places only.

Positive ion mode electrospray ionization mass spectrometry

Mass spectrometry of the IPC fraction (**Af-0**) was performed via electrospray ionization (ESI) in the positive ion mode ($^+$ESI) on a linear ion trap instrument (LTQ; Thermo-Finnigan, San Jose, CA). Mass spectrometry of all other fractions containing GIPCs was performed in the positive ion mode on a Micromass Global (Manchester, UK) hybrid ESI-Q/q-oa-TOF-MS instrument (Q-TOF). All (G)IPC samples were introduced into the ion source via direct infusion in 100% methanol (~100 ng/μl). The flow rate was usually 0.5 μl/min, but for analysis of samples available in limited amounts, a nanospray capillary tip was used, from which the flow rate was estimated to be ~200 nl/min. To generate $[M(Li)+Li]^+$ adducts of (G)IPC molecular species, LiI (10 mM) in methanol was added to the analyte solution until the observed ratio of $[M(Li)+Li]^+$ adducts to mixed Na^+/Li^+ adducts in MS profile mode was >5:1; the necessary LiI concentration was generally in the range 3–5 mM (39, 40). In general, spectra represent summations of 50–350 scans (30 scans/min) for MS $[M(Li)+Li]^+$ profiles and MS/collision-induced decomposition (CID)-MS (or LTQ MS^n) experiments. Resolution on the Q-TOF was generally 4,000 (5% valley) for MS profile spectra and 3,000 for MS/CID-MS experiments. Extraction cone voltage (analogous to orifice-to-skimmer potential in Sciex API series instruments) was 35 V for MS profile spectra and MS/CID-MS experiments and 80 V for pseudo-$^+$ESI-$(CID\text{-}MS)^2$ experiments. Additional matrix-assisted laser desorption time-of-flight (MALDI-TOF) mass spectrometry was performed on an Axima CFR (Shimadzu Biotech, Columbia, MD) instrument. Lithiation was accomplished by doping 2,5-dihydroxybenzoate matrix with LiI (41).

Fragment ion naming conventions and interpretation

Nominal, monoisotopic *m/z* values are used in the labeling and description of $^+$ESI-MS results. Fragment naming conventions and interpretation of spectra derived from $[M(Li)+Li]^+$ adducts of GIPC molecular species are based on those of Adams and Ann (42) and Singh, Costello, and Beach (43), as described previously (39–41); additional naming conventions for ceramide fragments are derived from Hsu and Turk (44). Essential characteristics of these spectra are summarized below with reference to **Scheme 2** (see also Schemes 3–7 below accompanying the mass spectra). In general, $^+$ESI-MS/CID-MS spectra of GIPCs acquired [via $^+$ESI-Q/q(CID)-oa-TOF-MS or other tandem MS/CID-MS configurations (30, 39–41)] from either disodiated or dilithiated molecular adducts exhibit abundant pairs of fragment ions representing the complete glycosylinositol ($[B_n+Cat]^+$ and $[C_n+Cat]^+$) and glycosylinositol phosphate ($[B_nPO_3(Cat)+Cat]^+$ and $[C_nPO_3(Cat)+Cat]^+$) moieties, along with ceramide ($[Y_0+Cat]^+$ and $[Z_0+Cat]^+$) and ceramide phosphate ($[Y_0PO_3(Cat)+Cat]^+$ and $[Z_0PO_3(Cat)+Cat]^+$) ions. Ions in parallel series, representing glycosidic fragmentations occurring singly or in combination with other cleavages, are also observed ($[C_n+Cat]^+$, $[B_n+Cat]^+$, $[Y_n+Cat]^+$, $[Z_n+Cat]^+$, $[Y_m/C_n+Cat]^+$, $[Y_m/B_n+Cat]^+$, $[Y_m/C_nPO_3(Cat)+Cat]^+$, and $[Y_m/B_nPO_3(Cat)+Cat]^+$). In many cases, these are accompanied by related $[Z_m/B_nPO_3(Cat)+Cat]^+$ and $[Z_m/B_n+Cat]^+$ ions. It has been found that the $[Y_m/C_nPO_3(Cat)+Cat]^+$ and $[Y_m/B_nPO_3(Cat)+Cat]^+$ series are the most useful fragments for deducing glycosidic sequences, because the presence of the phosphate moiety clearly labels the inositol-containing reducing end of the glycan, so that monosaccharide cleavages must yield losses from the nonreducing end. In general, $^+$ESI-MS/CID-MS or $^+$ESI-MS^n of $[M(Li)+Li]^+$ adducts of GIPCs appear to yield better overall *S/N* than $[M(Na)+Na]^+$ adducts (39–41).

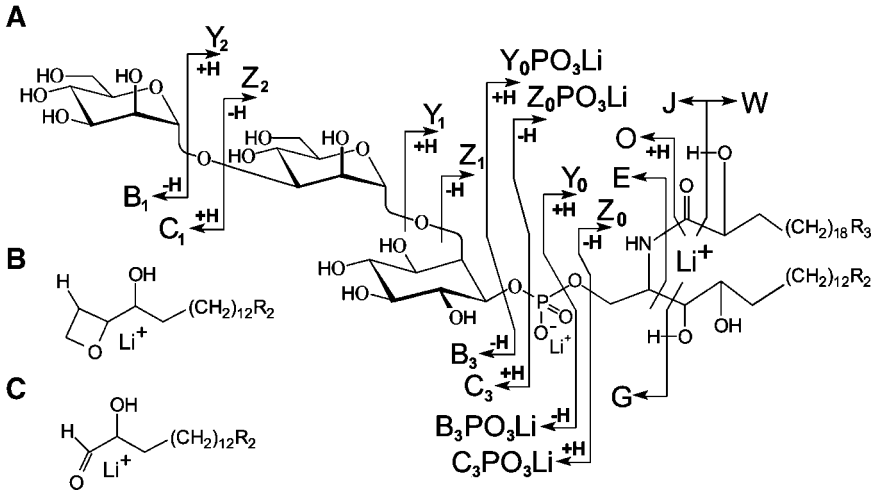

Scheme 2. Characteristic fragmentations of glycosylated IPCs, exemplified by Mα3Mα2IPC. A: Nomenclature based on that of Adams and Ann (42) for fragmentation of ceramide moiety and of Singh, Costello, and Beach (43) for glycosyl-*myo*-inositol phosphoryl group. B, C: Hydrated analogs of sphingoid d_{3b} and c_{1b} ions [nomenclature of Hsu and Turk (44)], proposed as products of t18:0 or t20:0 phytosphingosine-containing ceramides (39–41).

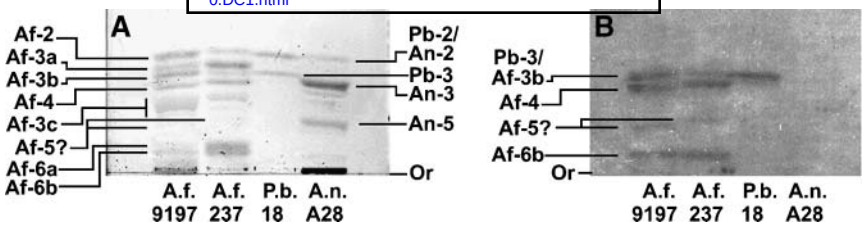

Fig. 1. High-performance thin-layer chromatography (HPTLC) immunostaining of crude fungal glycosylinositol phosphorylceramide (GIPC) fractions by monoclonal antibody MEST-1. A: Orcinol staining. B: MEST-1 immunostaining. Crude acidic fractions are as follows: lane 1, *A. fumigatus* (A.f.) strain 9197; lane 2, *A. fumigatus* strain 237; lane 3, *P. brasiliensis* (P.b.) strain 18; lane 4, *A. nidulans* strain A28.

Monosaccharide, inositol, fatty acid, sphingoid, and linkage analysis by GC-MS

Monosaccharides were analyzed as their per-*O*-trimethylsilyl methyl glycosides. A re-*N*-acetylation step was used after methanolytic depolymerization to ensure that hexosamines, if present, would be detected as their acetamido derivatives. Ceramide-derived sphingoid bases and 2-hydroxy fatty acids were detected as their *N*-acetyl-per-*O*-trimethylsilyl and 2-*O*-trimethylsilyl methyl ester derivatives, respectively. *Myo*-inositol (Ins) was detected in the monosaccharide analysis as its per-*O*-trimethylsilyl derivative, although optimal conditions for its release (20) were not used. All derivatives were prepared according to protocols described previously (30). Linkage analysis was performed by the method of partially methylated alditol acetates. Permethylation was performed by microscale adaptation of the method of Ciucanu and Kerek (45); hydrolysis, reduction, and acetylation to produce partially methylated alditol acetates were performed as described by Levery and Hakomori (46). Instruments used for GC-MS were a GCQ (Thermo-Finnigan) and a GC3800-MS1200 (Varian), operated in electron ionization mode. All component analyses were performed on a 30 m DB-5 (or equivalent) bonded-phase fused silica capillary column, temperature programmed from 160°C to 200°C at 2°/min and from 200°C to 260°C at 10°/min (for per-*O*-trimethylsilyl methyl glycosides) or from 140°C to 320°C at 4°/min (for fatty acid methyl esters and *N*-acetyl-per-*O*-trimethylsilyl sphingosines). Partially methylated alditol acetates were analyzed with the same system, temperature programmed from 160°C to 260°C at 2°/min. All derivatives were identified by comparison of retention times and mass spectra compared with authentic standards and published data.

RESULTS

Preliminary comparison of the immunoreactivity of *A. fumigatus* and *A. nidulans* GIPCs with monoclonal antibody MEST-1

In **Fig. 1** are reproduced HPTLC profiles of crude fungal acidic lipid fractions stained with orcinol (panel A), which reacts with hexose residues characteristic of GIPCs, and the monoclonal antibody MEST-1 (panel B), which specifically recognizes terminal Gal*f*β residues (25).[2] These compare the reactivity profiles of GIPCs from *A. fumigatus* strains 9197 and 237 (cultured at 37°C; lanes 1 and 2, respectively) with those from *P. brasiliensis* strain 18 (lane 3) and *A. nidulans* strain A28 (lane 4). The characterizations of the components from *P. brasiliensis* and *A. nidulans* have been described previously (30, 40), except that the component formerly named **Pb-1** is here named **Pb-3**.[3] The structural basis for naming the component bands from *A. fumigatus* will be described below. The *P. brasiliensis* antigen **Pb-3** [Man*p*(α1→3)[Gal*f*(β1→6)]Man*p*(α1→2)InsPCer], but not **Pb-2** [Man*p*(α1→3)Man*p*(α1→2)InsPCer], was previously observed to react with MEST-1 (25). The branching Gal*f*(β1→6) residue is known to be essential for the MEST-1 reactivity of **Pb-3**. Here, comigrating bands corresponding to **Af-3b** and **Pb-3** from *A. fumigatus* and *P. brasiliensis*, respectively, are both clearly stained with MEST-1 (Fig. 1B, lanes 1–3), suggesting that **Af-3b** may have a structure similar or identical to that of **Pb-3**. Interestingly, bands corresponding to **Af-4** from both strains of *A. fumigatus* also reacted, along with at least two other components with lower R_f in each strain. This suggests that **Af-4** contains the common branching Gal*f*(β1→6) residue responsible for MEST-1 reactivity. No other components of *P. brasiliensis* appeared to be reactive with MEST-1 (Fig. 1B, lane 3). No GIPC components from *A. nidulans* reacted (Fig. 1B, lane 4), as expected, because they have been shown to have divergent oligo-α-mannosyl structures without Gal*f*β (40). **Af-3a** appears to be unstained by MEST-1; although this is not completely clear because of the small difference in R_f with respect to **Af-3b**, the result would be consistent with absence, or unreactive presentation, of the Gal*f*β residue.

Fractionation of major *A. fumigatus* GIPCs

The HPTLC results in **Fig. 2A** compare crude acidic lipid fractions from *A. nidulans* strain A28 (lane 1) and *A. fumigatus* strain 237 (lane 2), cultured at 30°C, with a reference standard containing Manα3Manα2IPC (M_2IPC = **Pb-2**) and Gal*f*β6(Manα3)Manα2IPC (G_fM_2IPC = **Pb-3**) from *P. brasiliensis* (lane 3). Note that the component with

[2] An abbreviated structural notation is used in the Results and Discussion sections of this paper, wherein the pyranose ring form is assumed unless otherwise designated (e.g., Gal*f* = galactofuranosyl); in many cases, the anomeric carbon number, arrow, and parenthesis denoting linkage are assumed and omitted [e.g., Man*p*(α1→3)Man*p*(α1→2)Ins = Manα3Manα2Ins]. In some cases, Man may be further abbreviated as M, Ins as I, and Cer as C.

[3] We previously designated the *P. brasiliensis* GIPCs Manα3Manα2IPC and Manα3(Gal*f*β6)Manα2IPC as Pb-2 and Pb-1, respectively (30), but here we refer to them as **Pb-2** and **Pb-3**, respectively, correlating systematically with the number of monosaccharide residues in each and their retention factor (R_f) values in HPTLC.

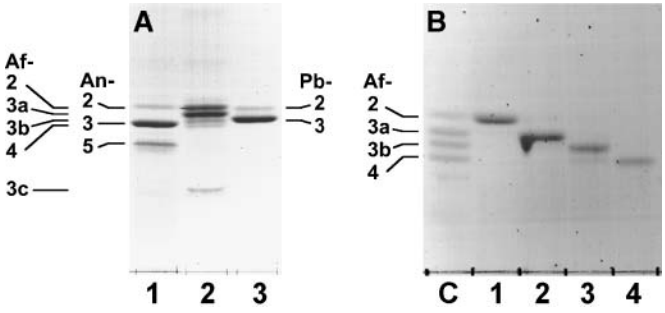

Fig. 2. A: HPTLC analysis comparing GIPC profiles (as orcinol-stained acidic lipid components) of *A. nidulans* strain A28 (lane 1) and *A. fumigatus* strain 237 (lane 2) alongside a mixture of GIPCs (Pb-2 and Pb-3) previously isolated and characterized from *P. brasiliensis* (lane 3). Note that *P. brasiliensis* component Pb-3 was previously referred to as Pb-1 (30) but is here redesignated according to the number of monosaccharide residues in its structure. *A. nidulans* components An-2, An-3, and An-5 were characterized previously by Bennion et al. (40). B: HPTLC analysis showing four major GIPCs in a profile of *A. fumigatus* strain 9197 (lane C), which were subsequently isolated as individual components (lanes 1–4) by repetitive HPLC fractionation. Designations of bands are given beside the panels, corresponding to relative R_f values and the number of monosaccharide residues found in each component. Mobile phases are as follow: panel A, chloroform-methanol-water [50:47:14 (v/v/v), containing 0.038% (w/v) $CaCl_2$]; panel B, chloroform-methanol-water [50:55:19 (v/v/v), containing 0.046% (w/v) $CaCl_2$].

the highest R_f value (**Af-2**) comigrated with authentic M_2IPC components previously characterized from *P. brasiliensis* (**Pb-2**) (30) and *A. nidulans* (**An-2**) (40), but the most abundant component (second band, **Af-3a**) had a slightly higher R_f than the other major GIPC from *P. brasiliensis* (**Pb-3**). A third, less abundant component (**Af-3b**) migrated at the same R_f as **Pb-3**, and the fourth band (**Af-4**) had a slightly lower R_f, consistent with three to four monosaccharide units attached to IPC. **Af-3b** and **Af-4** appeared to migrate, respectively, slightly above and slightly below the major GIPC component of *A. nidulans*, Manα6(Manα3)Manα2IPC (M_3IPC = **An-3**) (40). A fifth component, designated **Af-3c**, exhibiting a much lower R_f value by HPTLC, appeared in some preparations with a higher R_f and, as was discovered later, sometimes appeared in the neutral (DEAE-Sephadex pass-through) fraction. The reason for this, that it is a zwitterionic GIPC component, will be discussed below. Acidic lipids from strain 9197 exhibited a qualitatively similar profile, but with less **Af-3a** and more **Af-3b** and **Af-4** (data not shown). This *A. fumigatus* acidic fraction appeared to lack some of the additional low R_f components that were observed when the fungus was cultured at 37°C (see above).

Crude acidic lipids from both strains 237 and 9197 were fractionated by preparative-scale HPLC, with each of the first four major GIPC components obtained in at least one fraction as a single orcinol-stained band (Fig. 2B, lanes 1–4); these components, designated **Af-2**, **Af-3a**, **Af-3b**, and **Af-4**, respectively, were subjected to characterization by ^{1}H-NMR, MS, and GC-MS techniques as described below. An amount of **Af-3c** sufficient for extensive 2-D NMR analysis was accumulated from three HPLC fractionations of crude neutral lipids. An additional component, eluting before **Af-2** in HPLC but not stained by orcinol, was also collected and analyzed (it will be referred to as **Af-0**). Some intermediate fractions were found to be mixtures; analysis of such mixtures also produced useful results, as reported below.

Monosaccharide, inositol, fatty acid, and sphingoid component analysis of *A. fumigatus* GIPCs

Mannose was essentially the only monosaccharide identified by GC-MS analysis of the trimethylsilylated methyl glycosides produced after methanolysis of **Af-2** components from strains 237 or 9197. The **Af-3a** (237) fraction was observed to consist mainly of mannose, although a trace of galactose was also detected. **Af-3b** (9197) contained both galactose and mannose in an ~1:2 ratio. In **Af-3c**, 2-deoxy-2-amino-glucose was detected (as *N*-acetylglucosamine), along with mannose, in a ratio of ~1:2. Ins was detected in all four fractions. The major long-chain fatty acid detected was h24:0, identified by its characteristic retention time and fragments observed in its electron ionization mass spectrum (47). Small amounts of non-hydroxylated 16:0, 18:0, and 24:0 fatty acids were also detected, along with traces of h25:0, h26:0, and the dihydroxy fatty acid 2h24:0. Major sphingoid components detected were t18:0 and t20:0 4-hydroxysphinganines (phytosphingosines), in ratios varying between the different fractions. Under conditions of ion trap detection, electron ionization spectra of the 4-hydroxysphinganine-derived *N*-acetyl-1,3,4-tri-*O*-trimethylsilyl-4-hydroxysphinganines were qualitatively similar in most respects than those described previously by Thorpe and Sweeley (48), but with more abundant representation of high *m/z* ions, including some additional molecular mass-related ions as observed by Levery et al. (30). Thus, $[M-15]^+$, $[M-15-90]^+$, $[M-59-90]^+$, $[M-174]^+$, and $[M-174-90]^+$ ions were observed in high abundance at *m/z* 560, 470, 426, 401, and 311 for the t18:0 base derivative and at *m/z* 588, 498, 454, 429, and 329 for the later-eluting t20:0 base derivative (data not shown; for detailed interpretations, including identifications of lower *m/z* ions, see Refs. 48–50).

Structural analysis of *A. fumigatus* IPC (Af-0)

A partial 1-D ^{1}H-NMR spectrum of fraction **Af-0**, reproduced in Fig. 2, exhibited resonances characteristic for a Ins spin system as well as downfield resonances characteristic of the highly hydroxylated portion of phytoceramide, which we previously observed in GIPCs, but no resonances were observed characteristic for monosaccharide residues. Upfield resonances (data not shown) included a composite multiproton alkyl/acyl CH_2 signal at ~1.23 ppm and a characteristic 6H triplet for both the alkyl and acyl CH_3 at 0.853 ppm. Therefore, this fraction appears to contain IPC, the obligate intermediate in GIPC synthesis. The resonances were assigned as shown in **Fig. 3** and **Table 1**. The resonances assigned to Ins H-1 and

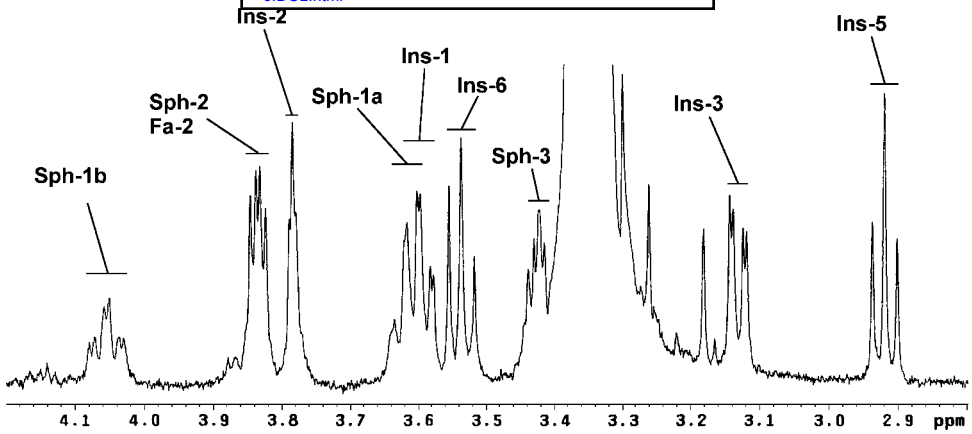

Fig. 3. Downfield expansion (4.20–2.80 ppm) of one-dimensional (1-D) ^{1}H-NMR spectra (500 MHz; DMSO-d_6/2% D_2O; 35°C) of the inositol phosphorylceramide (IPC) fraction (**Af-0**) isolated from *A. fumigatus* strain 9197.

Sph-1a/1b all exhibited additional three-bond coupling to the phosphorus atom of the phosphodiester (Table 1).

Because NMR analysis is less useful for determining ceramide size and relative sphingoid/fatty-*N*-acyl chain length distributions, the **Af-0** fraction was further analyzed by $^{+}$ESI-MS^{n} in a linear ion trap (**Fig. 4**). Two major lipoforms were detected as a pair of $[M(Na)+Na]^{+}$ salt-adduct ions observed at *m/z* 970 and 998, consistent with IPC having ceramides consisting of t18:0 and t20:0 4-hydroxysphinganines in combination with h24:0 fatty-*N*-acylation (Fig. 4A). To confirm that the *m/z* 28 (C_2H_4) increment is in the sphingoid and not the fatty-*N*-acyl moiety, further MS^{n} steps were carried out to isolate and fragment the ceramide ions; because we have observed that phytoceramide ions are somewhat difficult to generate and fragment under low-energy conditions but that fragmentation is facilitated by lithium adduction (39–41), the fraction was first treated with excess LiI and reinfused into the ESI source. As shown in Fig. 4B, this resulted in essentially complete conversion to a pair of predominant $[M(Li)+Li]^{+}$ adducts at *m/z* 938 and 966. MS^{2} product ion spectra (data not shown) of these two molecular adducts yielded highly abundant ceramide primary fragments $[Y_0+Li]^{+}$ at *m/z* 690 and 718, respectively, from losses of $[InsOPO_2(Li)-H]$ (with back transfer of H, as shown in Scheme 2). MS^{3} spectra of the $[Y_0+Li]^{+}$ ions at *m/z* 690 (Fig. 4C, *m/z* 938→690→) and 718 (Fig. 4D, *m/z* 966→718→) yielded products consistent with t18:0 and t20:0 4-hydroxysphinganines, respectively, as the major sphingoid components in the two lipoforms. Aside from the loss of H_2O from the $[Y_0+Li]^{+}$ ions (*m/z* 672 and 700 in Fig. 4C, D, respectively), the most abundant fragments were those corresponding to loss of the acyl chain ($[N+Li]^{+} \equiv [O/Y_0+Li]^{+}$) and a sphingoid rearrangement including additional loss of the amino group (d_{3b}), as observed previously in other low-energy fragmentation modes (Scheme 2, structure B) (39–41). These ions are observed at *m/z* 324 and 291 in the spectrum from *m/z* 690 (Fig. 4C) and at *m/z* 352 and 319 in the spectrum of products from *m/z* 718 (Fig. 4D), confirming that the *m/z*

TABLE 1. ^{1}H chemical shifts (ppm) for monosaccharide, inositol, ceramide sphingoid, and fatty-*N*-acyl (in parentheses) residues of IPC (*myo*-Ins1←P→1Cer = **Af-0**) and Manα3Manα2IPC (**Af-2**) from *A. fumigatus* in DMSO-d_6/2% D_2O at 35°C

Af-0	Ins	$J_{i,j}$ (Ins)	Cer	$J_{i,j}$ (Sph)
H-1	3.599	$^{3}J_{1,2}$ = 2.5, $^{3}J_{1,P}$ = 9.8	3.616 (a), 4.054 (b)	$^{2}J_{1a,1b}$ = 10.4, $^{3}J_{1a,P}$ = 9.4, $^{3}J_{1b,P}$ = 10.0
H-2	3.784	$^{3}J_{2,3}$ = 2.5	3.834 (3.834)	$^{3}J_{1a,2}$ = 7.2; $^{3}J_{1b,2}$ = 3.7
H-3	3.130	$^{3}J_{3,4}$ = 9.7	3.422	
H-4	3.37	$^{3}J_{4,5}$ = 8.9	—	
H-5	2.918	$^{3}J_{5,6}$ = 8.7	—	
H-6	3.536	$^{3}J_{6,1}$ = 9.7	—	
Af-2	Manα3	Manα2	Ins	Cer
H-1	4.895	5.062	3.732	3.640, 4.044
($^{3}J_{1,2}$)	(∼1.5–2.0)	(∼1.5–2.0)	—	
H-2	3.732	3.919	3.968	3.846 (3.825)
H-3	3.585	3.654	3.229	3.458
H-4	3.449	3.609	3.350	3.352
H-5	3.575	3.904	2.945	
H-6	3.615	3.553	3.496	
H-6'	3.512	3.492	—	

Ins, *myo*-inositol; IPC, inositol phosphorylceramide. $^{3}J_{1,2}$ (Hz) for monosaccharide residues are given in parentheses; glycosidically linked ^{13}C are given in boldface.

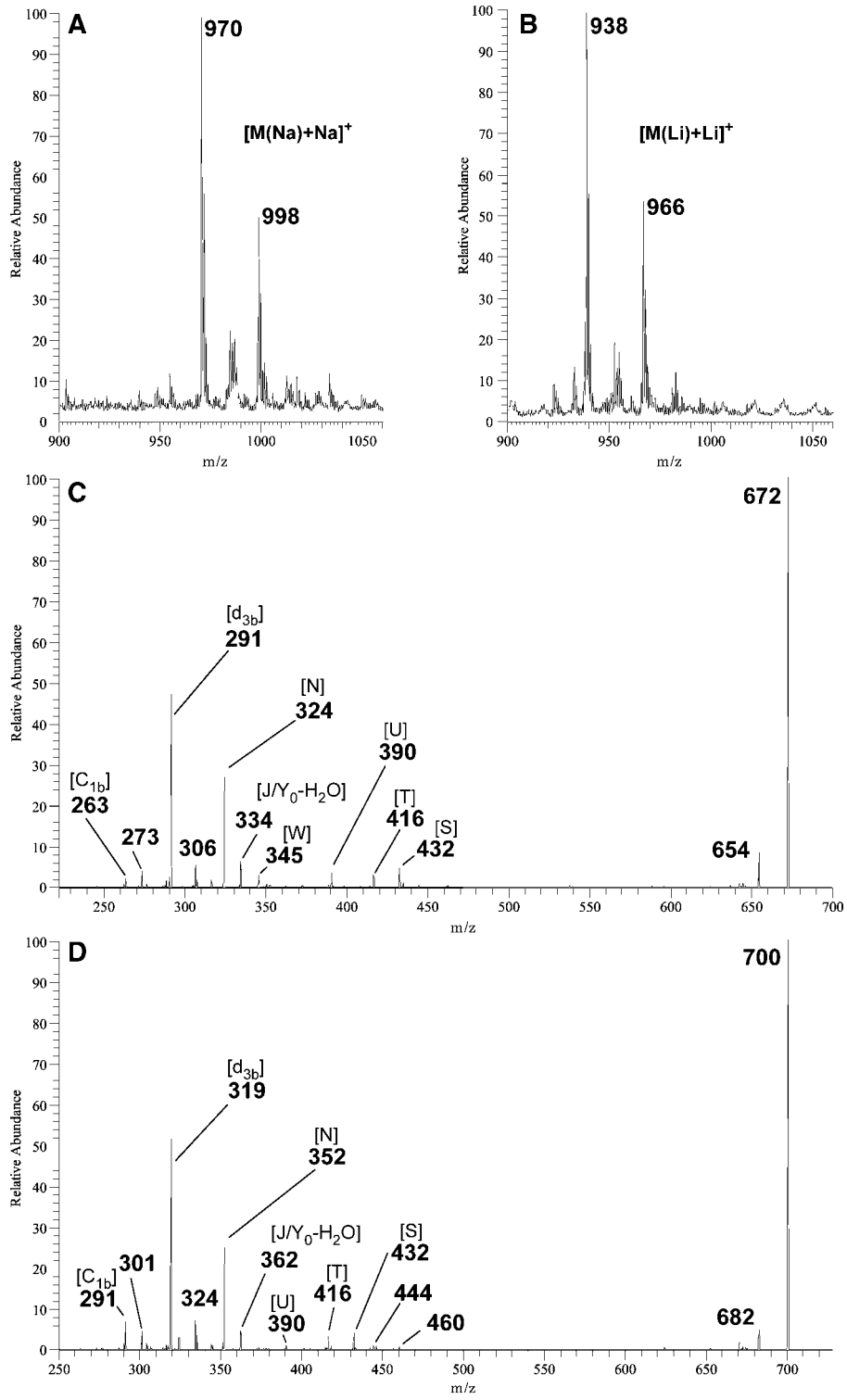

Fig. 4. Positive ion mode electrospray ionization ($^{+}$ESI-MS^{n}) spectra of **Af-0**. A: Profile of molecular ions as $[M(Na)+Na]^{+}$ adducts. B: Profile of molecular ions as $[M(Li)+Li]^{+}$ adducts. C: MS^{3} products of the $[Y_0+Li]^{+}$ primary fragment at *m/z* 690 (*m/z* 938→690→). D: MS^{3} products of $[Y_0+Li]^{+}$ at *m/z* 718 (*m/z* 966→718→). The adduct designation "+Li" and the charge form have been omitted from the fragment labels for clarity.

28 differences in the ceramide moieties reside entirely in the sphingoid chain lengths, whereas the *N*-acyl group is h24:0 in both ceramide species. Minor products included ions derived from these by dehydration or further fragmentation. Ions derived from the loss of all or most of the sphingoid alkyl chain, while retaining the fatty-*N*-acyl chain (e.g., *m/z* 432 $[S+Li]^{+}$, 416 $[T+Li]^{+}$, and 390 $[U+Li]^{+}$), as well as an aldehyde ion derived from the fatty-*N*-acyl C_2-C_ω (*m/z* 345 $[W+Li]^{+}$), are observed at the same *m/z* in both spectra (Scheme 2).

Structural analysis of *A. fumigatus* GIPCs

Af-2 from strains 237 and 9197. A 1-D ^{1}H-NMR spectrum of an **Af-2** fraction from strain 237 is reproduced in **Fig. 5A**. Aside from the presence of minor impurities, it is essentially identical to a spectrum previously published for Manα3Manα2IPC (Pb-2) from *P. brasiliensis* and for which most of the resonances were assigned by 2-D homonuclear COSY and TOCSY experiments (30). For confirmation, **Af-2** was subjected to a similar sequence of 2-D ^{1}H-NMR analyses; the resonance assignments are listed for reference in Table 1. Key points are the α-Man anomeric resonances observable at 5.062 ppm (Manα2 H-1) and 4.896 ppm (Manα3 H-1); the corresponding α-Man H-2 resonances at 3.919 and 3.732 ppm, respectively; Ins H-2, H-3, and H-5 resonances at 3.968, 2.945, and 3.230 ppm, respectively; sphingoid H-1b and H-2 resonances at 4.044 and 3.837, respectively; and the fatty-*N*-acyl H-2 resonance at 3.845 ppm. Note that the α-mannosylation at Ins O-2 correlates with downfield shift increments for the Ins H-1, H-2, and H-3 resonances with respect to their values in InsPCer ($\Delta\delta$ = 0.13, 0.18, and 0.10 ppm, respectively), consistent with increments found by comparison with data previously reported for Manα2InsPCer (22). The minor anomeric resonances at 5.030 and 4.905 ppm are consistent with a small contamination by a triglycosyl-IPC component (see below) incompletely separated from **Af-2** in this fraction. A 1-D ^{1}H-NMR spectrum of the **Af-2** component from strain 9197 was of somewhat lower quality, but it lacked contamination from the triglycosyl-IPC component (data not shown). All of the salient features discussed above were visible in this spectrum, confirming its identity to the Manα3Manα2IPC isolated from strain 237.

For further characterization, particularly of the ceramide moiety, which could differ from those of other species and is not well defined by NMR methods, a molecular profile of **Af-2** from strain 9197 was acquired via $^+$ESI-Q/oa-TOF-MS. These data are described in detail in

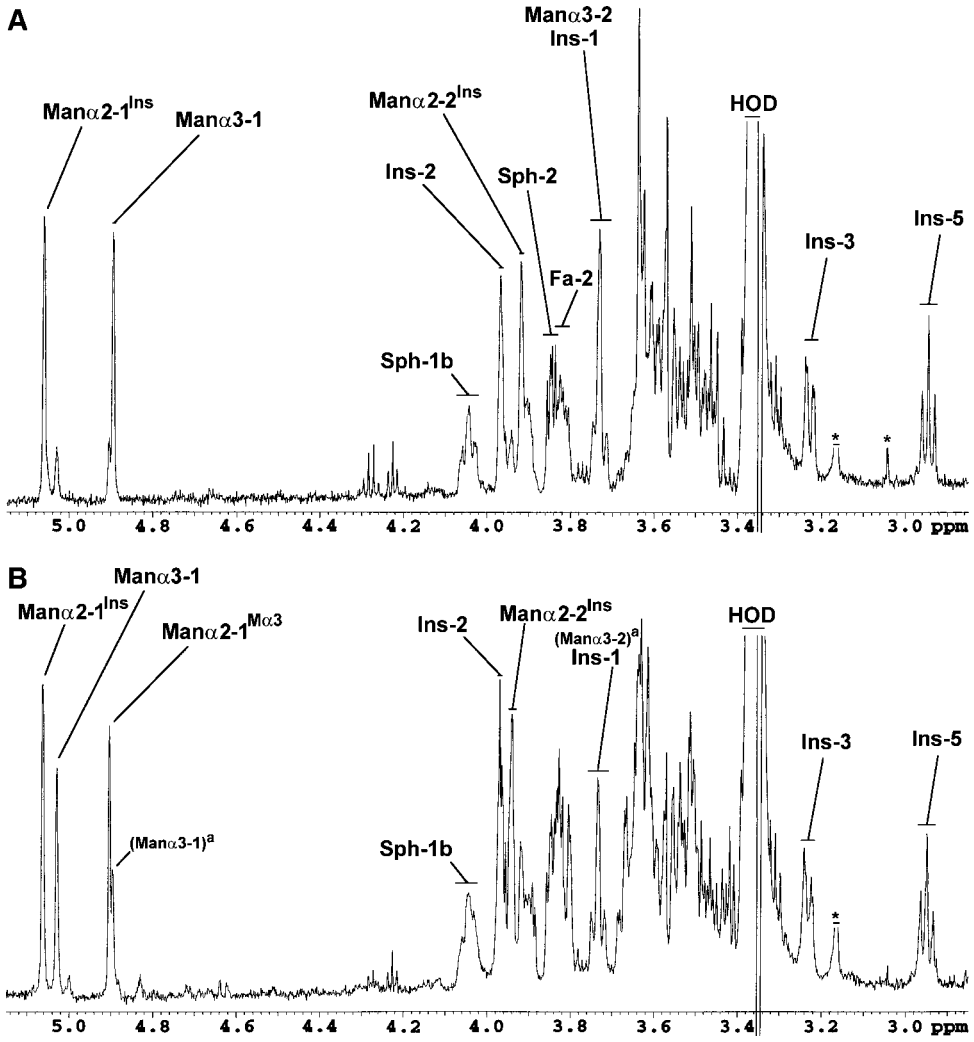

Fig. 5. Downfield expansion (5.15–2.85 ppm) of 1-D ^{1}H-NMR spectra (800 MHz; DMSO-d_6/2% D_2O; 35°C) of GIPC fractions isolated from *A. fumigatus* strain 237. Spectra were acquired on fractions corresponding to lanes 1 and 2 of Fig. 1B. A: **Af-2**. B: **Af-3a**. Resonances denoted by parentheses are assigned to protons of residual **Af-2** in the sample.

the supplementary data (supplementary Figs. I, II and Scheme I). These results were consistent with an M_2IPC having ceramides consisting of t18:0 and t20:0 4-hydroxysphinganines with h24:0 fatty-*N*-acylation and minor lipoforms with compositions h25:0/t18:0 and h24:0/t19:0.

Af-3a from strain 237. The 1-D ^{1}H-NMR spectrum of a fraction of **Af-3a** (Fig. 5B) showed it to be not a homogeneous GIPC component but a mixture of **Af-2** and an additional triglycosyl-IPC having a set of three anomeric protons at 4.905, 5.029, and 5.064 ppm. The anomeric protons from **Af-2** are observed as lower intensity signals at 4.897 and 5.064 ppm, the latter coincident with one of the signals from the major triglycosyl-IPC component, as indicated by the greater relative intensity of that signal. Conversely, resonances from the major **Af-3a** component are observable as minor signals in the spectrum of **Af-2** from strain 237 (cf. Fig. 5A). Unfortunately, because of the insufficient amount and the presence of two closely related structures in the mixture, we were not able to obtain high-quality 2-D NMR data specific for the **Af-3a** component from this fraction, resulting in only fragmentary resonance assignments. Signals assignable by apparent analogy were Ins H-3 and H-5 resonances at 2.948 and 3.231 ppm, respectively; sphingoid H-1b and H-2 reso-

TABLE 2. Comparison of ^{1}H chemical shifts (ppm) for H-1 of monosaccharide residues of Manα3Manα2IPC (**Af-2**), Manα2Manα3Manα2IPC (**Af-3a**), Manα3(Gal*f*β6)Manα2IPC (**Af-3b**), and Manα2Manα3(Gal*f*β6)Manα2IPC (**Af-4**) from *A. fumigatus* in DMSO-d_6/2% D_2O at 35°C

	Man*p*α1→2Manα1→3(Gal*f*β1→6)Manα1→2*myo*-Ins1←P→1Cer			
Af	Manα2	Manα3	(Gal*f*β6)	Manα2
Af-2	—	4.895	—	5.062
Af-3a	4.905	5.029	—	5.064
Af-3b	—	4.889	4.828	5.005
Af-4	4.901	5.023	4.826	5.000

Glycosidically linked ^{13}C are given in boldface.

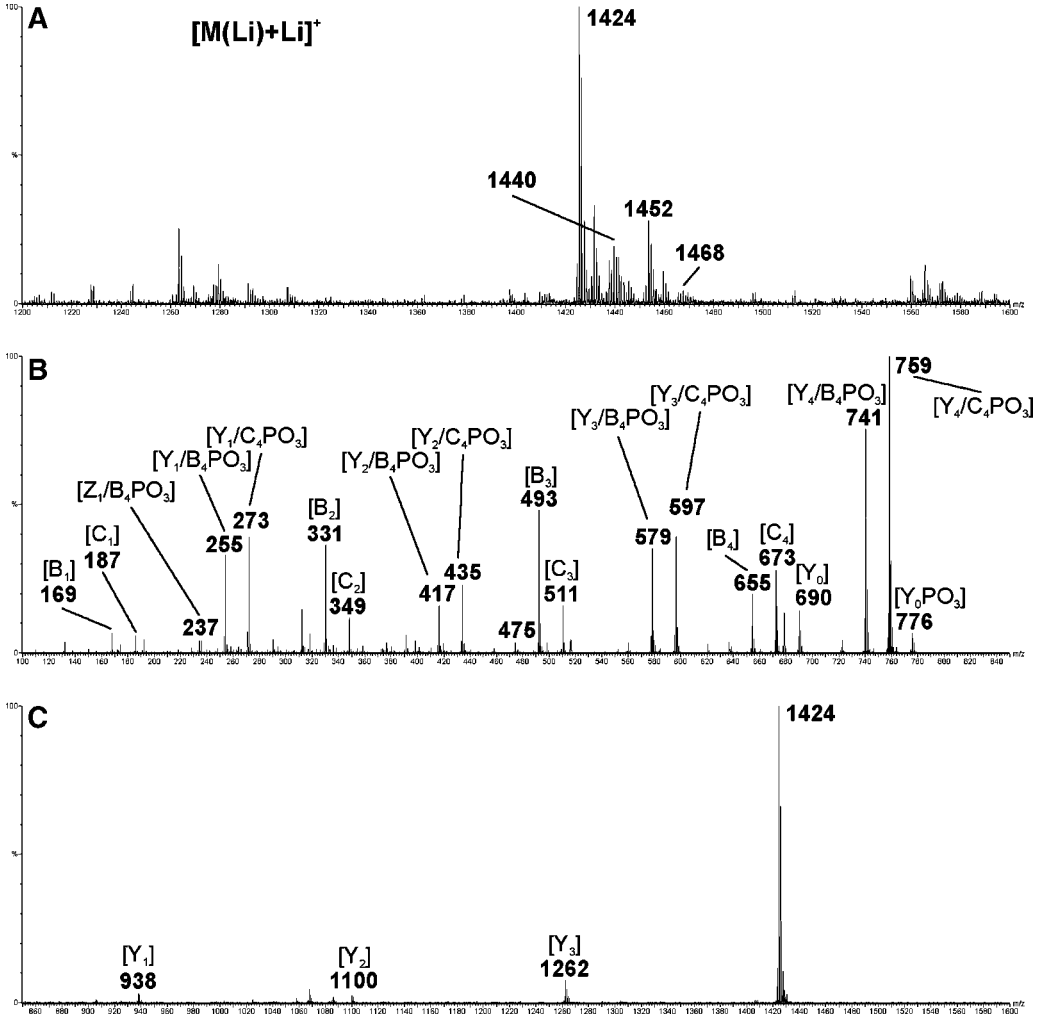

Fig. 6. $^+$ESI-Qq/oa-TOF spectra of **Af-3a**. A: Profile of molecular ions as $[M(Li)+Li]^+$ adducts. B: MS/collision-induced decomposition (CID)-MS of $[M(Li)+Li]^+$ at *m/z* 1,424, low *m/z* region. C: MS/CID-MS of $[M(Li)+Li]^+$ at *m/z* 1,424, high *m/z* region. The y axis expansion in C relative to B is 27×. Ion designations correspond to Scheme 4. The designations "+Li" and "(Li)+Li" and the charge form have been omitted from the fragment labels for clarity.

nances at 4.047 and 3.847, respectively; and a fatty-*N*-acyl H-2 resonance at 3.827 ppm. The similarity in chemical shift of two of the H-1 signals to those of **Af-2** suggested that it could be a derivative of Manα3Manα2IPC, although potential glycosylation-induced changes in chemical shifts preclude reliable assignments based purely on analogy. A triglycosyl structure consisting solely of α-Man*p* residues would be consistent with the similar $^{3}J_{1,2}$ values (1.5–2.0 Hz) of all H-1 resonances observed in the spectrum.

A linkage analysis by GC-MS detected derivatives corresponding to T-Man, →3Man, and →2Man. The first two derivatives would be produced from the **Af-2** known to be present, but the latter, assuming that **Af-3a** is a mannosylated product of **Af-2**, as the NMR data suggest, would only be consistent with addition of the third Man residue in 1→2 linkage. Such a structure would also produce the same T-Man and →3Man derivatives. Therefore, the structure Manα2Manα3Manα2IPC is proposed for **Af-3a**. This structure could be consistent with the NMR spectrum, provided that the signal at 5.029 ppm is assigned to H-1 of the penultimate Manα3 residue, because it is known that glycosylation of an α-Man residue by Manα2 induces a substantial downfield shift of H-1 of the substituted residue (51). The resonance at 4.905 ppm, therefore, is assigned to H-1 of the nonreducing terminal Manα2 residue, with H-1 of the reducing end Manα2 residue remaining at 5.064 ppm, apparently unaffected by the substitution (**Table 2**).

A molecular profile of **Af-3a** was acquired via $^{+}$ESI-Q/oa-TOF-MS (**Fig. 6A**); a pair of $[M(Li)+Li]^{+}$ salt-adduct ions observed at *m/z* 1,424 and 1,452 is consistent with a triglycosyl-IPC having ceramides consisting of t18:0 and t20:0 4-hydroxysphinganines and h24:0 fatty-*N*-acylation. A $^{+}$ESI-MS/CID-MS spectrum acquired from the dilithiated molecular adduct at *m/z* 1,424 is reproduced in Fig. 6B, C, showing the predominant $[B_3PO_3(Li)+Li]^{+}$/$[C_3PO_3(Li)+Li]^{+}$ pair (*m/z* 741/759) and other abundant fragments from glycosidic cleavages (**Scheme 3**). In addition to glycosidic fragment series derived from the glycosylinositol phosphate and glycosylinositol moieties, fragments from sequential loss of monosaccharide residues from $[M(Li)+Li]^{+}$ ($[Y_m(Li)+Li]^{+}$) appear at lower abundance in the spectrum. In the same region of the spectra and at similar abundance, ions from loss of the acyl chain and loss of acyl C_2-C_ω ($[O(Li)+Li]^{+}$, $[J(Li)+Li]^{+}$, and $[J'(Li)+Li]^{+}$) are also observed (Scheme 2). Within this group, the latter ion appears to be predominant. Similar to previous results, the ceramide and ceramide phosphate ions ($[Y_0+Li]^{+}$, $[Z_0+Li]^{+}$, $[Y_0PO_3(Li)+Li]^{+}$, and $[Z_0PO_3(Li)+Li]^{+}$) appear at intermediate abundances. The $[O(Li)+Li]^{+}$, $[J(Li)+Li]^{+}$, $[J'(Li)+Li]^{+}$, and $[O/Z_0PO_3(Li)+Li]^{+}$ ions all provide information about the carbon number of the sphingoid and, by difference, the *N*-acyl chain, all or part of which is lost in the process of their formation. A similar spectrum was acquired from the $[M(Li)+Li]^{+}$ adduct at *m/z* 1,452 (data not shown), differing only in the *m/z* of sphingoid-containing fragments. Thus, in agreement with the sphingoid and fatty acid analysis, these spectra indicate that the *m/z* 28 increment between the two predominant molecular species is attributable primarily to a corresponding C_2H_4 difference in the sphingoid rather than the *N*-acyl chain. Therefore, the $[M(Li)+Li]^{+}$ adducts at *m/z* 1,424 and 1,452 correspond to lipoforms containing t18:0 and t20:0 4-hydroxysphinganines, respectively, with h24:0 fatty-*N*-acylation.

Af-3b from strain 9197. The 1-D ^{1}H-NMR spectrum of fraction **Af-3b** showed it to be a nearly homogeneous GIPC component, although a few major peaks from non-GIPC

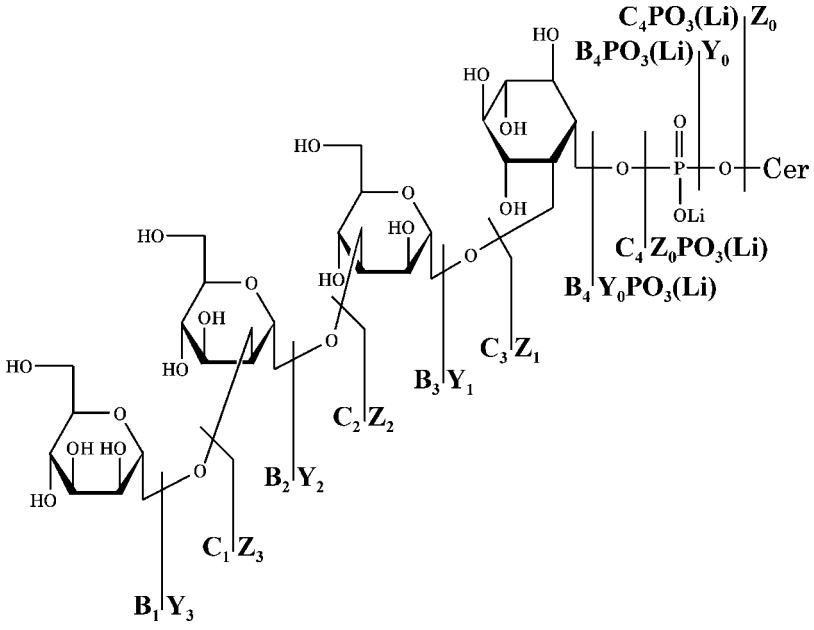

Scheme 3. Fragmentation of **Af-3a** in positive ion mode ESI-MS and ESI-MS/CID-MS.

impurities could be observed (data not shown). Three anomeric proton resonances are clearly observed in the downfield region of the spectrum (**Fig. 7A**) at 5.005 ppm ($^3J_{1,2} < 2.0$ Hz), 4.889 ppm ($^3J_{1,2} < 2.0$ Hz), and 4.828 ppm ($^3J_{1,2} = 2.0$ Hz). These values are almost identical to those previously observed for the branched Gal*f*β6-containing triglycosyl-IPC isolated from *P. brasiliensis*, Manα3(Gal*f*β6)Manα2IPC (30), referred to here as **Pb-3**. This structure would be consistent with its HPTLC R_f value and immunoreactivity toward MEST-1 (see below). There were some differences in the spectra, however. These could be attributable to impurities, but to be more certain of the resonance and structure assignments, a series of 2-D ^{1}H-^{1}H and ^{13}C-^{1}H spectra were acquired, because off-diagonal correlations originating from H-1 resonances in 2-D ^{1}H-^{1}H spectra of glycoconjugates can generally be assigned in the presence of obscuring impurity peaks, and from these monosaccharide ring ^{1}H spin system assignments most ^{13}C-^{1}H correlations can then be interpreted.

Thus, almost all monosaccharide, inositol, and ceramide resonances were unambiguously assignable from 2-D ^{1}H-^{1}H gCOSY and TOCSY experiments (data not shown; **Table 3**). Analysis of approximate $^3J_{i,j}$ proton-coupling constants around the three monosaccharide spin systems confirmed the presence of two α-Man residues, particularly recognizable by their signature small values for $^3J_{1,2}$ and $^3J_{2,3}$. Definitive analysis of the β-Gal*f* spin system was more problematic, but it was characterized by its essentially identical appearance to that observed previously for this residue in **Pb-3** (30); acquisition of ^{13}C resonance NMR data (which had not been obtained previously) proved helpful in eliminating any doubt about the identity of this residue in particular (see below). Analysis of approximate $^3J_{i,j}$ coupling constants around the cyclic Ins spin system confirmed it as Ins (all hydroxyl groups equatorial except that at C-2), whereas the chemical shift pattern, compared with previously acquired data, was consistent with glycosylation of Ins at O-2 (22, 23, 30, 52). An interesting characterizing feature of the **Af-3b** ^{1}H-NMR spectral data is the downfield shift of the Manα2 H-5 (4.053 ppm), which was observed previously for **Pb-3** (30), as well as another GIPC having the Manα2 residue substituted at O-3 and O-6 [i.e., Manα3(Manα6)Manα2IPC (**An-3**) from *Aspergillus nidulans* (40)].

Finally, ^{13}C resonance assignments (Table 3), made from a 2-D ^{1}H-detected, ^{13}C-^{1}H gHSQC spectrum (data not shown), were also consistent with the linkage of two glycosyl α-Man*p* residues to the core Manα2 residue at O-3 and O-6; this is supported by a pattern of substantial downfield shift increments (α-effects) for Manα2 C-3 and C-6, along with upfield shift decrements (β-effects) (53) for Manα2 C-2, C-4, and C-5, compared with ^{13}C spectral data for the parent compound, Manα2IPC (22). A striking feature of the ^{13}C-NMR spectral data is the extreme downfield position of the C-1 resonance correlated with H-1 at 4.828 ppm; its chemical shift of 108.3 ppm essentially confirms the identification of a β-Gal*f* residue (53). All other ^{13}C chemical shifts are consistent with the proposed Manα2IPC core structure, including those characteristic for the Ins residue substituted at O-2 (22, 40). Based on all of these data, the structure of **Af-3b** was proposed with high confidence to be Manα3(Gal*f*β6)Manα2IPC.

TABLE 3. ^{1}H and ^{13}C chemical shifts (ppm) for monosaccharide, inositol, ceramide sphingoid, and fatty-*N*-acyl (in parentheses) residues of Manα3(Gal*f*β6)Manα2IPC (**Af-3b**) from *A. fumigatus* in DMSO-d_6/2% D_2O at 35°C

Af-3b	Manα3	(Gal*f*β6)	Manα2	Ins	Cer
H-1	4.889	4.828	5.005	3.726	3.660, 4.035
($^3J_{1,2}$)	(<2.0)	(<2.0)	(2.0)	—	
H-2	3.731	3.827	3.924	3.980	3.830 (3.840)
H-3	3.587	3.798	3.641	3.213	3.456
H-4	3.448	3.492	3.578	3.377	3.352
H-5	3.587	3.396	4.053	2.963	
H-6	3.617	3.413	3.770	3.500	
H-6′	3.524	3.378	3.456	—	
C-1	102.0	108.3	101.0	75.9	64.4
C-2	70.7	81.3	69.6	**77.8**	50.4 (74.0)
C-3	71.0	77.0	**78.6**	70.7	73.2
C-4	67.3	71.2	64.6	72.0	70.6
C-5	73.6	73.9	72.0	75.7	
C-6	61.1	63.0	**66.9**	72.5	

$^3J_{1,2}$ (Hz) for monosaccharide residues are given in parentheses; glycosidically linked ^{13}C are given in boldface.

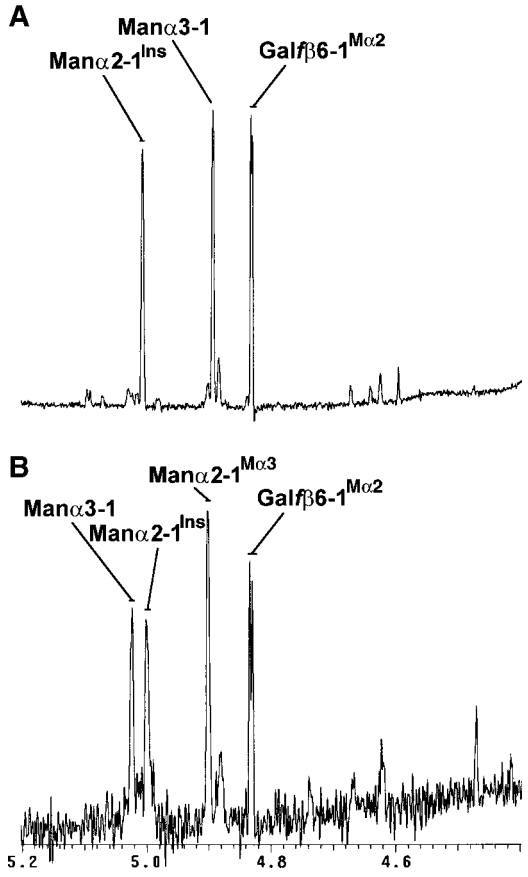

Fig. 7. Downfield expansion of the anomeric proton region (5.2–4.4 ppm) of 1-D ^{1}H-NMR spectra (500 MHz; DMSO-d_6/2% D_2O; 35°C) of GIPC fractions isolated from *A. fumigatus* strain 9197. A: **Af-3b**. B: **Af-4**. Spectra were acquired on fractions corresponding to lanes 3 and 4 of Fig. 1B.

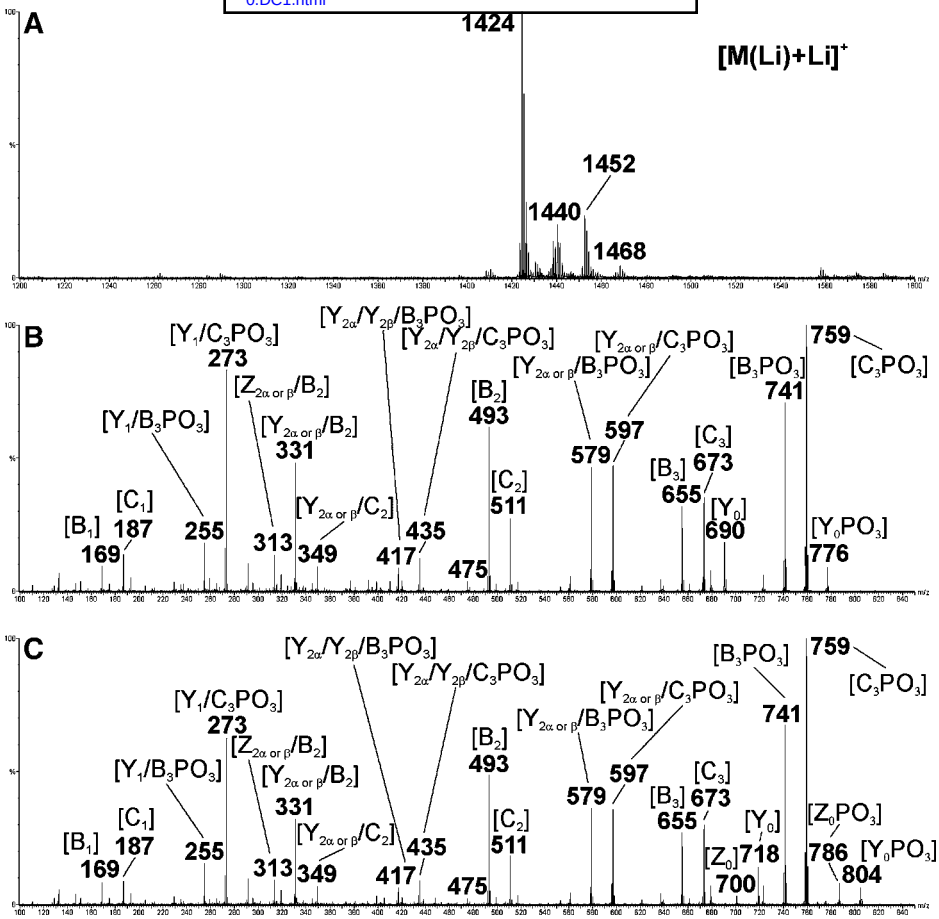

Fig. 8. $^{+}$ESI-Qq/oa-TOF spectra of **Af-3b**. A: Profile of molecular ions as $[M(Li)+Li]^{+}$ adducts. B: MS/CID-MS of $[M(Li)+Li]^{+}$ at *m/z* 1,424, low *m/z* region. C: MS/CID-MS of $[M(Li)+Li]^{+}$ at *m/z* 1,452, low *m/z* region. Ion designations correspond to Scheme 5. The designations "+Li" and "(Li)+Li" and the charge form have been omitted from the fragment labels for clarity.

A molecular profile of **Af-3b** was acquired via $^{+}$ESI-Q/oa-TOF-MS (**Fig. 8A**); a pair of $[M(Li)+Li]^{+}$ salt-adduct ions observed at *m/z* 1,424 and 1,452 is consistent with a triglycosyl-IPC having ceramides consisting of t18:0 and t20:0 4-hydroxysphinganines with h24:0 fatty-*N*-acylation. Lower *m/z* expansions of $^{+}$ESI-MS/CID-MS spectra acquired from the dilithiated molecular adducts at *m/z* 1,424 and 1,452 are reproduced in Fig. 8B, C, showing the predominant $[B_3PO_3(Li)+Li]^{+}/[C_3PO_3(Li)+Li]^{+}$ pair (*m/z* 741/759) and other abundant fragments. Similar to

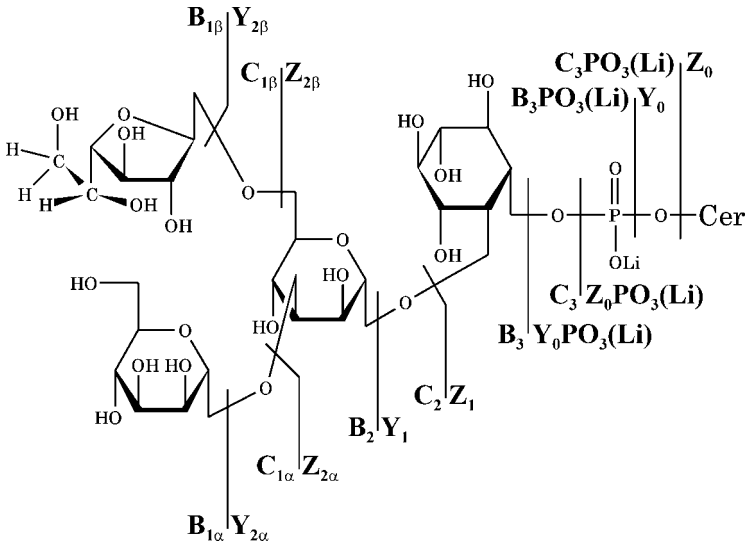

Scheme 4. Fragmentation of **Af-3b** in positive ion mode ESI-MS and ESI-MS/CID-MS.

other GIPC components discussed, fragments from sequential loss of monosaccharide residues from $[M(Li)+Li]^+$ ($[Y_m(Li)+Li]^+$), as well as ions from loss of the acyl chain and loss of acyl C_2-C_ω ($[O(Li)+Li]^+$, $[J(Li)+Li]^+$, and $[J'(Li)+Li]^+$), were also observed at lower abundance in higher *m/z* regions of the spectra (data not shown). As described above, the ceramide and ceramide phosphate ions ($[Y_0+Li]^+$, $[Z_0+Li]^+$, $[Y_0PO_3(Li)+Li]^+$, and $[Z_0PO_3(Li)+Li]^+$) appear at intermediate abundances. The $[O(Li)+Li]^+$, $[J(Li)+Li]^+$, $[J'(Li)+Li]^+$, and $[O/Z_0PO_3(Li)+Li]^+$ ions (data not shown) all agreed with the sphingoid and fatty acid analysis, which indicates that the *m/z* 28 increment between the two predominant molecular species is primarily attributable to a corresponding C_2H_4 difference in the sphingoid rather than the *N*-acyl chain. Thus, the $[M(Li)+Li]^+$ adducts at *m/z* 1,424 and 1,452 again correspond to lipoforms containing t18:0 and t20:0 4-hydroxysphinganines, respectively, with h24:0 fatty-*N*-acylation.

Inspection of the series of fragments derived by glycosidic bond cleavages from the $[B_3PO_3(Li)+Li]^+/[C_3PO_3(Li)+Li]^+$ pair showed that, consistent with previous findings (39–41), a somewhat lower abundance is observed for glycosylinositol phosphate fragment ions requiring at least two glycosidic cleavages for their appearance ($[Y_{2\alpha}/Y_{2\beta}/B_3PO_3(Li)+Li]^+$ and $[Y_{2\alpha}/Y_{2\beta}/C_3PO_3(Li)+Li]^+$, at *m/z* 417 and 435, respectively), compared with other ions in the $[Y_m/B_nPO_3(Li)+Li]^+$ and $[Y_m/C_nPO_3(Li)+Li]^+$ series, indicating the presence of a branch point in the glycan (**Scheme 4**). In particular, the ratios of the relative abundances of *m/z* 435 versus *m/z* 273 (0.14), and *m/z* 435 versus *m/z* 597 (0.25), are attenuated by factors of 5 and 2, respectively, in **Af-3b** compared with the same ratios in the isomeric unbranched **Af-3a** (0.70 and 0.52, respectively). Reductions in these abundance ratios have been observed previously for branched GIPCs under these conditions; although the precise magnitudes of such reductions are not identical to those observed here, the trends are very similar (40).

Af-4 from strain 9197. In the downfield 1-D ^{1}H-NMR spectrum of fraction **Af-4** (Fig. 7B), four major anomeric proton signals can be observed at 4.826, 4.901, 5.000, and 5.023 ppm (all $^3J_{1,2} \sim 1.5$–2.0 Hz), suggesting that it represents a tetraglycosyl-IPC. Two of these chemical shifts (4.901 and 5.023) are similar to those observed for H-1 resonances of **Af-3a**, whereas the other two (4.826 and 5.000) are similar to those observed for H-1 resonances of **Af-3b**, suggesting that it might contain features common to both triglycosyl-IPCs. In terms of glycosylation-induced chemical shift changes for the H-1 resonances, **Af-4** could be thought of as having the same relationship with **Af-3a** as **Af-3b** has with **Af-2** (addition of branching Gal*f*β6 to the Manα3 residue), or the same relationship with **Af-3b** as **Af-3a** has with **Af-2** (addition of terminal Manα2 to the Manα3 residue); for this reason, the structure Manα2 Manα3(Gal*f*β6)Manα2IPC was proposed.

A molecular profile of **Af-4** was acquired via $^+$ESI-Q/oa-TOF-MS (**Fig. 9A**); a pair of $[M(Li)+Li]^+$ salt-adduct

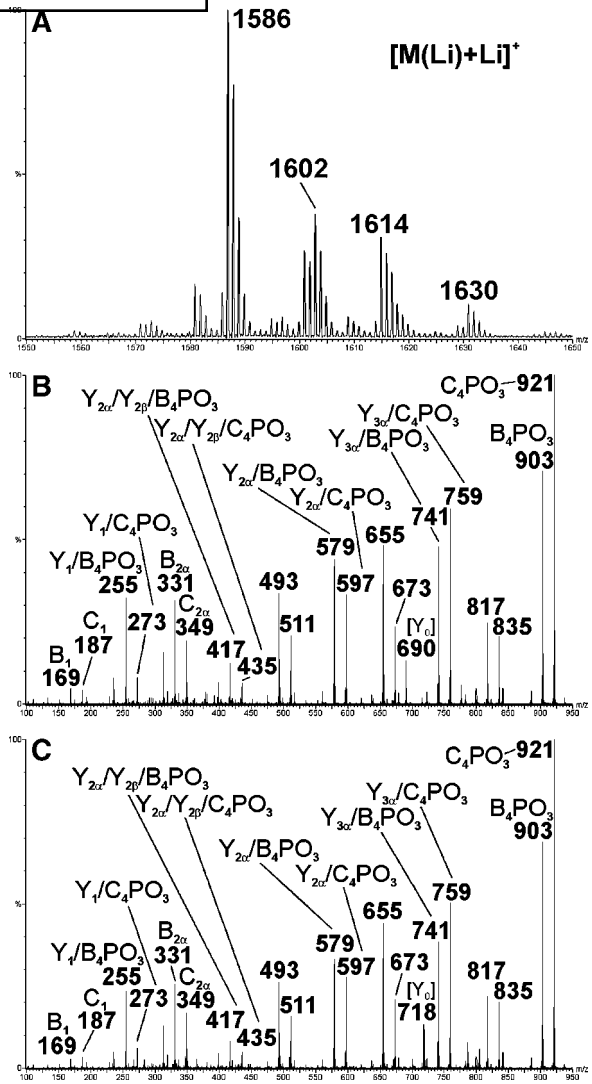

Fig. 9. $^+$ESI-Qq/oa-TOF spectra of **Af-4**. A: Profile of molecular ions as $[M(Li)+Li]^+$ adducts. B: MS/CID-MS of $[M(Li)+Li]^+$ at *m/z* 1,586, low *m/z* region. C: MS/CID-MS of $[M(Li)+Li]^+$ at *m/z* 1,614, low *m/z* region. Ion designations correspond to Scheme 5. The designations "+Li" and "(Li)+Li" and the charge form have been omitted from the fragment labels for clarity.

ions observed at *m/z* 1,586 and 1,614 is consistent with a tetraglycosyl-IPC having ceramides consisting of t18:0 and t20:0 4-hydroxysphinganines with h24:0 fatty-*N*-acylation. Other ions in the profile at *m/z* 1,602 and 1,630 yielded spectra consistent with mixed $[M(Na)+Li]^+$ salt adducts (indicating somewhat inadequate LiI addition, but not affecting conclusions drawn from the fully lithiated molecular ions). Lower *m/z* expansions of $^+$ESI-MS/CID-MS spectra acquired from the dilithiated molecular adducts at *m/z* 1,424 and 1,452 are reproduced in Fig. 9B, C, showing the predominant $[B_4PO_3(Li)+Li]^+/[C_4PO_3(Li)+Li]^+$ pair (*m/z* 903/921) and other abundant fragments. Similar to other GIPC components discussed, fragments from sequential loss of monosaccharide residues from $[M(Li)+Li]^+$ ($[Y_m(Li)+Li]^+$), as well as ions from loss of the acyl chain and loss of acyl C_2-C_ω ($[O(Li)+Li]^+$, $[J(Li)+Li]^+$, and $[J'(Li)+Li]^+$), were also observed at

lower abundance in higher *m/z* regions of the spectra (data not shown). As described above, the ceramide and ceramide phosphate ions ($[Y_0+Li]^+$, $[Z_0+Li]^+$, $[Y_0PO_3(Li)+Li]^+$, and $[Z_0PO_3(Li)+Li]^+$) appear at intermediate abundances. The $[O(Li)+Li]^+$, $[J(Li)+Li]^+$, $[J'(Li)+Li]^+$, and $[O/Z_0PO_3(Li)+Li]^+$ ions (data not shown) all agreed with the sphingoid and fatty acid analysis, which indicates that the *m/z* 28 increment between the two predominant molecular species is primarily attributable to a corresponding C_2H_4 difference in the sphingoid rather than the *N*-acyl chain. Thus, the $[M(Li)+Li]^+$ adducts at *m/z* 1,586 and 1,614 again correspond to lipoforms containing t18:0 and t20:0 4-hydroxysphinganines, respectively, with h24:0 fatty-*N*-acylation.

The low ratios of the relative abundances of *m/z* 435 versus *m/z* 597 (0.18) in both CID spectra appear to be consistent with a structure branched at the inner α-Man residue. Interestingly, however, the *m/z* 273 appeared to be highly attenuated with respect to its abundance in all other spectra acquired to date; the significance of this difference is unclear. In all other respects, the fragmentation spectra are consistent with the proposed structure of **Af-4**, Manα2Manα3(Gal*f*β6)Manα2IPC (**Scheme 5**).

Af-3c from strain 9197. A significant amount of this component was isolated from both the acidic and neutral fractions of *A. fumigatus* lipids. Component analysis by GC-MS indicated that the low-R_f fraction **Af-3c** contained mannose and glucosamine (detected as GlcNAc) in a 2:1 ratio; other components detected were Ins, t18:0 and t20:0 4-hydroxysphinganines (phytosphingosines), and h24:0 fatty acid (major). The relevant downfield section of a 1-D ^{1}H-NMR spectrum of fraction **Af-3c** (corresponding material isolated from neutral fraction lipids) is reproduced in **Fig. 10A**; a section of the TOCSY spectrum corresponding to this region is reproduced in Fig. 10B. These data show a marked similarity to those obtained previously for Manα3Manα6GlcNα2IPC (Ss-Y6) previously isolated and characterized from the yeast form of *Sporothrix schenckii* (23). We still consider this structure particularly unusual (see Discussion) and therefore sought to confirm its occurrence in this context with a thorough reanalysis of fraction **Af-3c**, supporting it with additional heteronuclear experiments not reported previously.

As described above, chemical shift/connectivity assignments of all ^{1}H signals, as well as approximate measurements of $^3J_{i,j}$ coupling constants, in the monosaccharide, inositol, and proximal part of the ceramide were obtained from sequential application of 2-D ^{1}H-^{1}H gradient-COSY and TOCSY experiments. Complete assignments of ^{1}H resonances derived from this analysis are listed in **Table 4**. The Ins residue is recognized as a cyclic spin system in which all $^3J_{i,j}$ are large except for $^3J_{1,2}$ and $^3J_{2,3}$, as H-2 is the only equatorial proton in the 1,2,3,4,5,6-hexahydroxycyclohexane ring. The three monosaccharide residues are recognized by their connectivity/coupling patterns, starting from the most downfield signal (H-1) of each spin system. Aside from the presence of two Man residues recognizable by their signature small values for $^3J_{1,2}$ and $^3J_{2,3}$, the NMR spectrum of **Af-3c** is characterized in particular as exhibiting a sugar H-2 signal shifted far upfield at 2.460 ppm, part of a spin system, originating from H-1 at 5.011 ppm, having $^3J_{i,j}$ coupling patterns consistent with an α-glucopyranosyl configuration. The upfield-shifted signal is consistent with H-2 attached to a carbon atom bearing an amino group, although in the *S. schenckii* GIPC, it was observed significantly farther upfield, at 2.380 ppm. The chemical shift of this proton

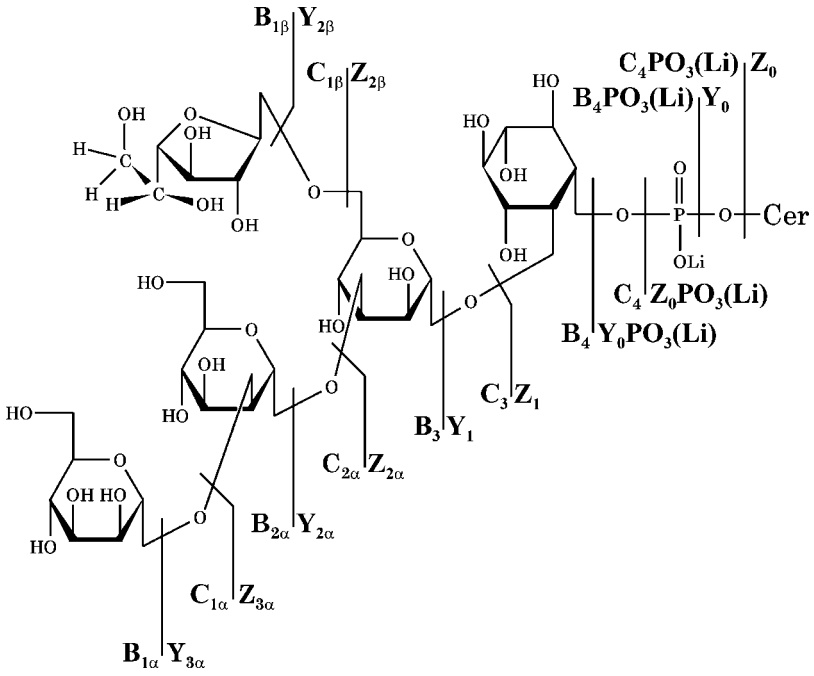

Scheme 5. Fragmentation of **Af-4** in positive ion mode ESI-MS and ESI-MS/CID-MS.

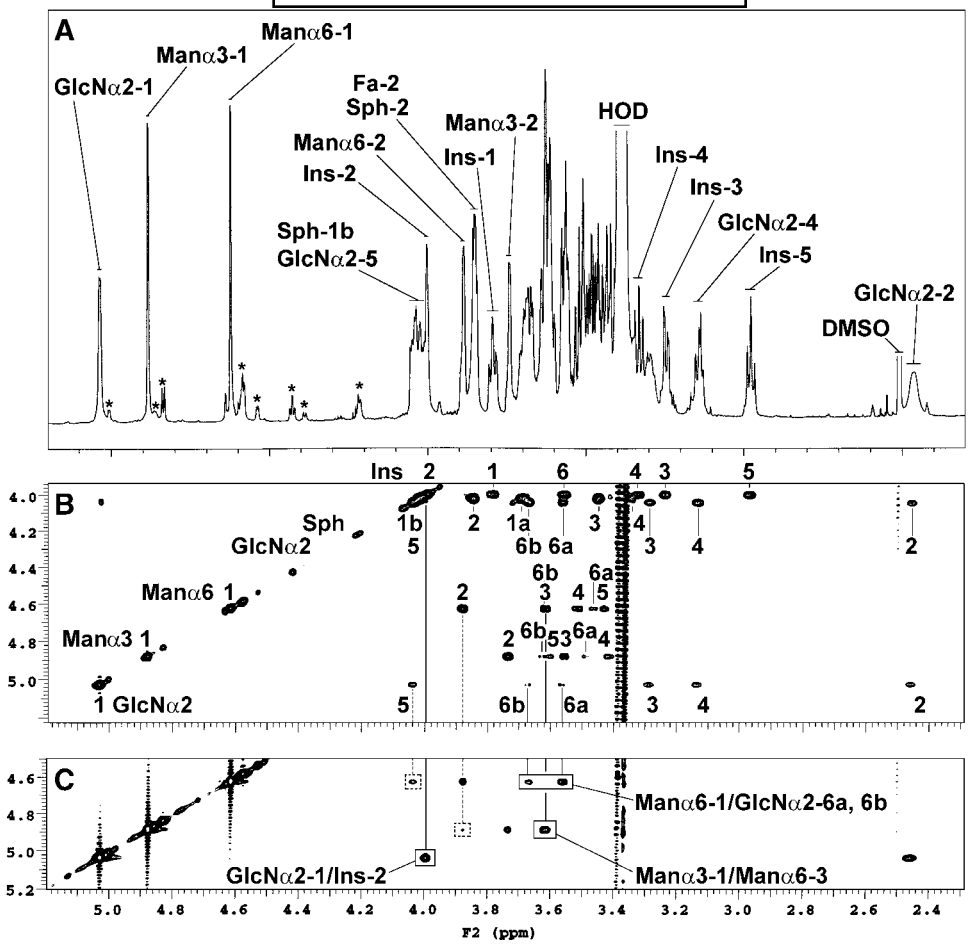

Fig. 10. Downfield expansion (F_2, 5.20–2.30 ppm) of 1-D and 2-D ^{1}H-NMR spectra (800 MHz; DMSO-d_6/2% D_2O; 35°C) of *A. fumigatus* GIPC fraction **Af-3c**. A: 1-D spectrum. B: Lower right section of 2-D ^{1}H-^{1}H total correlation spectroscopy (TOCSY) spectrum (200 ms mixing time; F_1, 5.22–3.94 ppm). C: 2-D ^{1}H-^{1}H nuclear Overhauser effect spectroscopy spectrum (200 ms mixing time; F_1, 5.20–4.50 ppm). In A, resonances marked with asterisks are from residual monosaccharide hydroxy protons; in B, TOCSY correlations originating from these resonances have been deleted for clarity. In C, interresidue nuclear Overhauser effect correlations directly across glycosidic linkages are boxed, weaker interresidue correlations are marked by dashed boxes, and intraresidue correlations have been left unmarked.

may reflect the zwitterionic status of the GIPC, because the spectral data were obtained from an **Af-3c** fraction isolated from the neutral fraction of *A. fumigatus* lipids, whereas in the case of the *S. schenckii* component reported previously, it was isolated from the anionic fraction (23). Presumably, in the latter case, the deprotonated amino form would have been isolated, which condition should be consistent with a more upfield shift of the vicinally linked proton, H-2, compared with that in the zwitterionic form, in which the amino group is protonated and therefore more electron-withdrawing.

The linkage assignments were established by observation in the nuclear Overhauser effect spectroscopy spectrum (Fig. 10C) of strong interresidue correlations between H-1 of the α-GlcN residue at 5.034 ppm and Ins H-2 (4.000 ppm), between α-Man H-1 at 4.622 ppm and α-GlcN H-6 (3.564 ppm), and between α-Man H-1 at 4.883 ppm and H-3 of the first α-Man residue (3.618 ppm). Weak interresidue correlations were also observed from α-Man H-1 to α-GlcN H-5 (4.040 ppm) and other H-6 (3.675 ppm). Further unambiguous confirmation of these linkages was obtained by collection of directly detected ^{13}C data and correlation of these with already assigned ^{1}H resonances via one-bond correlations observed in a 2-D ^{13}C-^{1}H-HSQC experiment (data not shown; Table 4). Relative downfield shifts of Ins C-2, GlcNα2 C-6, and Manα6 C-3 are consistent with glycosidic linkage points on those residues. In a subsequent ^{13}C-^{1}H-heteronuclear multiple bond correlation experiment (**Fig. 11**), a three-bond correlation was clearly observed between the α-GlcN H-1 resonance at 5.034 ppm and the uniquely assignable Ins C-2 resonance at 79.96 ppm. Additional three-bond correlations could be observed between the α-Man H-1 at 4.622 ppm and α-GlcN C-6 at 65.73 ppm and between the second α-Man H-1 at 4.883 ppm and C-3 of the first α-Man at 79.31 ppm.

In preliminary $^+$MALDI-TOF-MS analysis (data not shown), two major $[M(Na)+Na]^+$ salt-adduct ions for **Af-3c**

TABLE 4. ^{1}H and ^{13}C chemical shifts (ppm) for monosaccharide, inositol, ceramide sphingoid, and fatty-*N*-acyl (in parentheses) residues of Manα3Manα6GlcNα2IPC (**Af-3c**) from *A. fumigatus* in DMSO-d_6/2% D_2O at 35°C

Af-3c	Manα3	Manα6	GlcNα2	Ins	Cer
H-1	4.883	4.622	5.034	3.793	3.689, 4.021
($^{3}J_{1,2}$)	(<2.0)	(1.8)	(3.6)	—	—
H-2	3.741	3.882	2.460	4.000	3.849 (3.845)
H-3	3.555	3.618	3.295	3.241	3.455
H-4	3.422	3.512	3.135	3.329	3.350
H-5	3.602	3.428	4.040	2.974	
H-6	3.498	3.462	3.564	3.555	
H-6'	3.628	3.630	3.675	—	
C-1	102.49	100.12	100.12	75.83	64.48 (173.67)
C-2	70.60	69.64	56.49	**79.96**	50.60 (71.17)
C-3	71.43	**79.31**	74.07	70.60	73.20
C-4	67.42	66.06	70.24	72.64	70.60
C-5	73.72	74.07	71.12	75.70	
C-6	61.39[a]	61.27[a]	**65.73**	71.43	

$^{3}J_{1,2}$ (Hz) for monosaccharide residues are given in parentheses; glycosidically linked ^{13}C are given in boldface.
[a] May be interchanged.

were observed at *m/z* 1,455 and 1,483, in approximately equal abundance, consistent with a composition of Hex_2·HexN·Ins·P linked to predominant ceramides composed of t18:0 and t20:0 phytosphingosines with h24:0 fatty acid. Much less abundant molecular adducts, consistent with $[M(Na)+K]^+$ and $[M(K)+K]^+$ salt-adduct ions differing by +16 u increments from the major species, as well as $[M(Na)+H]^+$ ions differing from the major species by −22 u decrements, were also detectable. An aliquot of **Af-3c** was then subjected to conditions for selective *N*-acetylation and reanalyzed. In $^{+}$MALDI-TOF-MS, the two $[M(Na)+Na]^+$ salt-adduct ions were now observed abundantly at *m/z* 1,497 and 1,525, the +42 u increment consistent with the addition of one acetyl group to each of the major **Af-3c** lipoforms (data not shown). Less abundant pairs of ions were also observed in the spectrum at *m/z* 1,455 and 1,483, and at *m/z* 1,539 and 1,567, corresponding to unacetylated and over-*O*-acetylated species.

More detailed analysis was carried out via $^{+}$ESI-MS and $^{+}$ESI-MS/CID-MS of lithium salt adducts on the Q-TOF instrument (after treatment of the *N*-acetylated **Af-3c** sample with concentrated aqueous NH_3 to remove *O*-acetylated components). An $^{+}$ESI-MS profile now exhibited the two major $[M(Li)+Li]^+$ salt adduct ions for *N*-acetylated **Af-3c** at *m/z* 1,465 and 1,493 (**Fig. 12**). Corresponding $^{+}$ESI-MS/CID-MS product ion spectra were acquired with the selection of each molecular adduct precursor; the spectrum of products from *m/z* 1,465 is reproduced in Fig. 12). The glycosylinositol phosphate fragments $[C_4PO_3(Li)+Li]^+$ and $[B_4PO_3(Li)+Li]^+$ are now observed abundantly at *m/z* 800 and 782, respectively; the corresponding glycosylinositol fragments $[C_4+Na]^+$ and $[B_4+Na]^+$ are observed at *m/z* 714 and 696, respectively. Fragment ions arising from additional glycosidic cleavages of all four of these primary products are also observed in abundance in these spectra, especially significant being the phosphorylated ion series including *m/z* 255 ($[Y_1/B_4PO_3(Li)+Li]^+$) and 273 ($[Y_1/C_4PO_3(Li)+Li]^+$), 458 ($[Y_2/B_4PO_3(Li)+Li]^+$) and 476 ($[Y_2/C_4PO_3(Li)+Li]^+$), and 620 ($[Y_3/B_4PO_3(Li)+Li]^+$) and 638 ($[Y_3/C_4PO_3(Li)+Li]^+$). Again, the increment of *m/z* 203 between $[Y_1/\text{-}]$ and $[Y_2/C_4PO_3(Li)+Li]^+$ (or between $[Y_1/\text{-}]$ and $[Y_2/B_4PO_3(Li)+Li]^+$) clearly reflects the attachment of Glc(NAc) directly to the Ins residue (**Scheme 6**). The structure of **Af-3c** is thus clearly confirmed

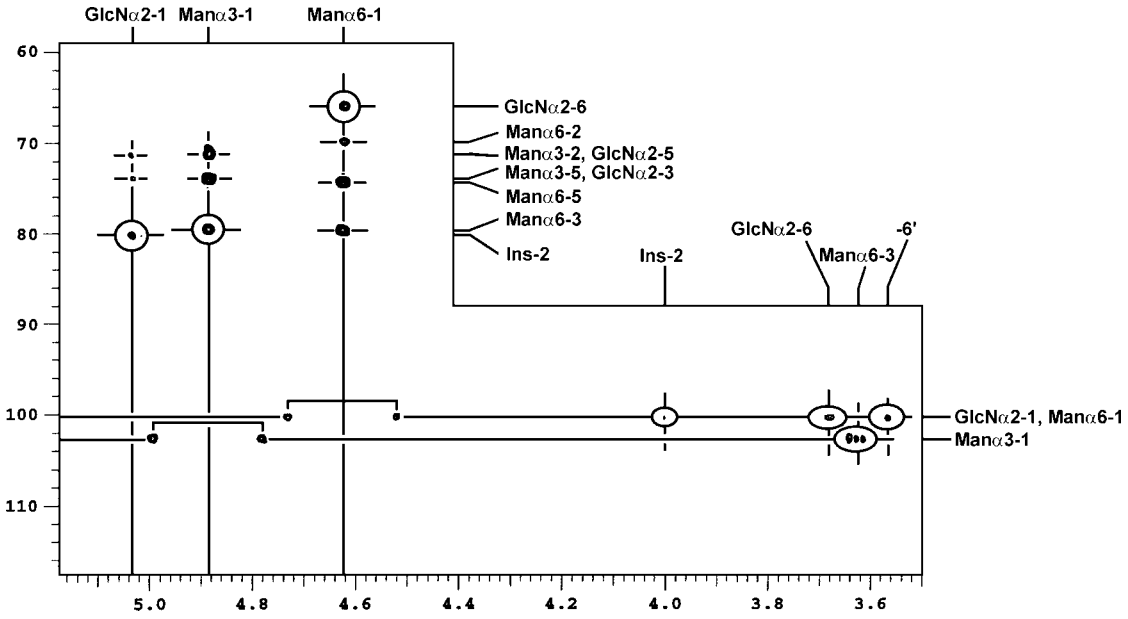

Fig. 11. Downfield expansion (F_2, 5.20–3.50 ppm; F_1, 120–60 ppm) of 2-D ^{1}H-detected ^{13}C-^{1}H-g heteronuclear multiple bond correlation spectrum (800 MHz; DMSO-d_6/2% D_2O; 35°C) of *A. fumigatus* GIPC fraction **Af-3c**. Interglycosidic three-bond ^{13}C-^{1}H correlations are circled and labeled with connectivities thus established.

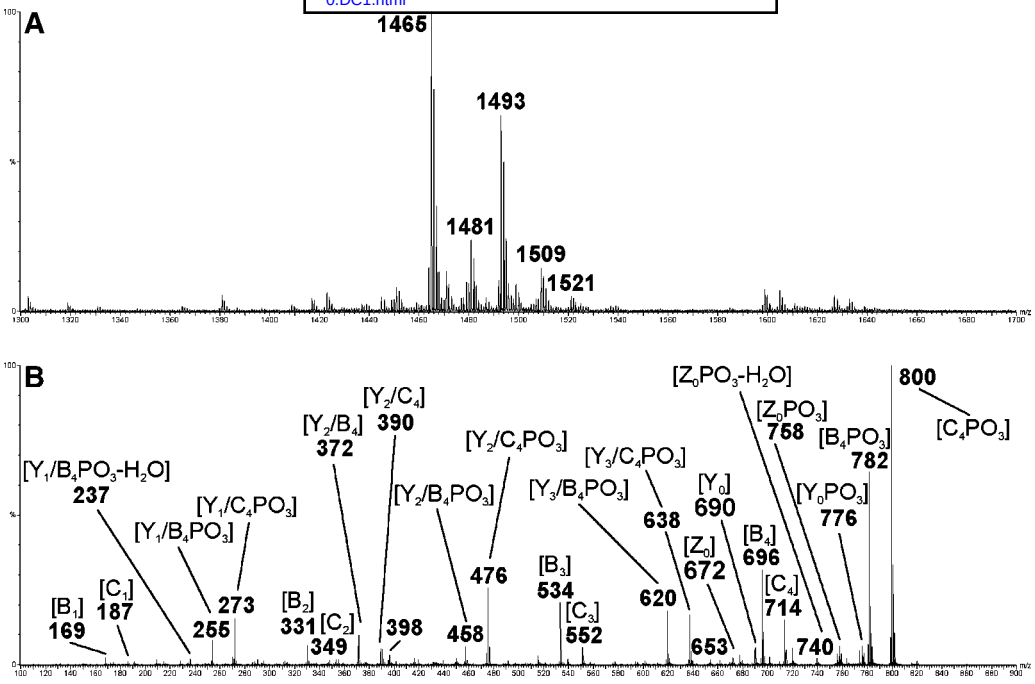

Fig. 12. $^{+}$ESI-Qq/oa-TOF spectra of *N*-acetylated **Af-3c**. A: Profile of molecular ions as $[M(Li)+Li]^{+}$ adducts. B: MS/CID-MS of $[M(Li)+Li]^{+}$ at *m/z* 1,465, low *m/z* region. Ion designations correspond to Scheme 6. The designations "+Li" and "(Li)+Li" and the charge form have been omitted from the fragment labels for clarity.

by the combination of NMR and mass spectrometric analysis as Manα3Manα6GlcNα2IPC.

Detection of *N*-acetylated Af-3c in strain 9197 GIPCs

During subsequent analysis of some impure fractions of *A. fumigatus* GIPCs, interpretation of an unexpected observation was greatly facilitated by the prior acquisition of extensive MS data on the *N*-acetylated derivative of **Af-3c**. Reproduced in **Fig. 13** is the molecular adduct ion profile acquired by $^{+}$ESI-MS on a fraction containing mainly **Af-2** but also apparently contaminated with lesser amounts of triglycosyl-IPC components. As expected, the most abundant $[M(Li)+Li]^{+}$ ions (*m/z* 1,262 and 1,290) are those consistent with **Af-2** being the major component (accompanying ions at +16 u increments are the result of underlithiation, yielding significant contribution of mixed salt-adduct species, $[M(Na)+Li]^{+}$ or $[M(Li)+Na]^{+}$). Their $^{+}$ESI-MS/CID-MS spectra were also consistent with

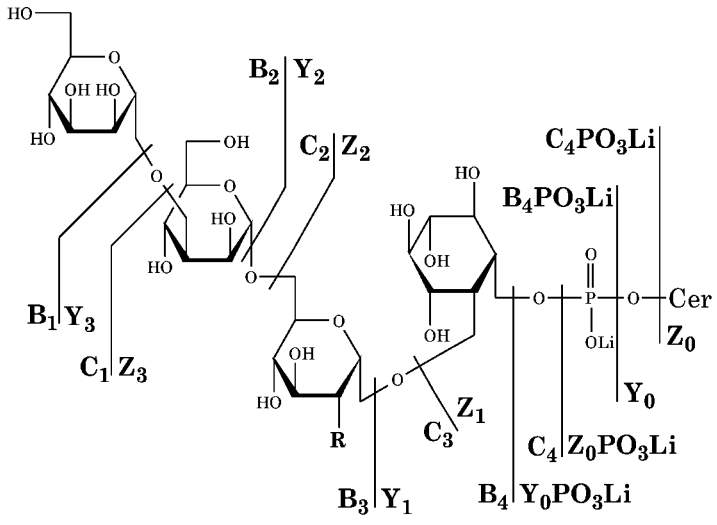

Scheme 6. Molecular ions and fragmentation of **Af-3c** and *N*-acetylated **Af-3c** in positive ion mode ESI-MS and ESI-MS/CID-MS. Phosphorylated fragments are labeled as Li^{+} salt adducts, but Na^{+} salt adducts can be named by substitution of Li with Na. Nominal, monoisotopic *m/z* values for both disodiated and dilithiated molecular species are given below the structure.

R=NH_2; $[M(Na)+Na]^{+}$=1455, 1483; $[M(Li)+Li]^{+}$=1423, 1451

R=NAc; $[M(Na)+Na]^{+}$=1497, 1525; $[M(Li)+Li]^{+}$=1465, 1493

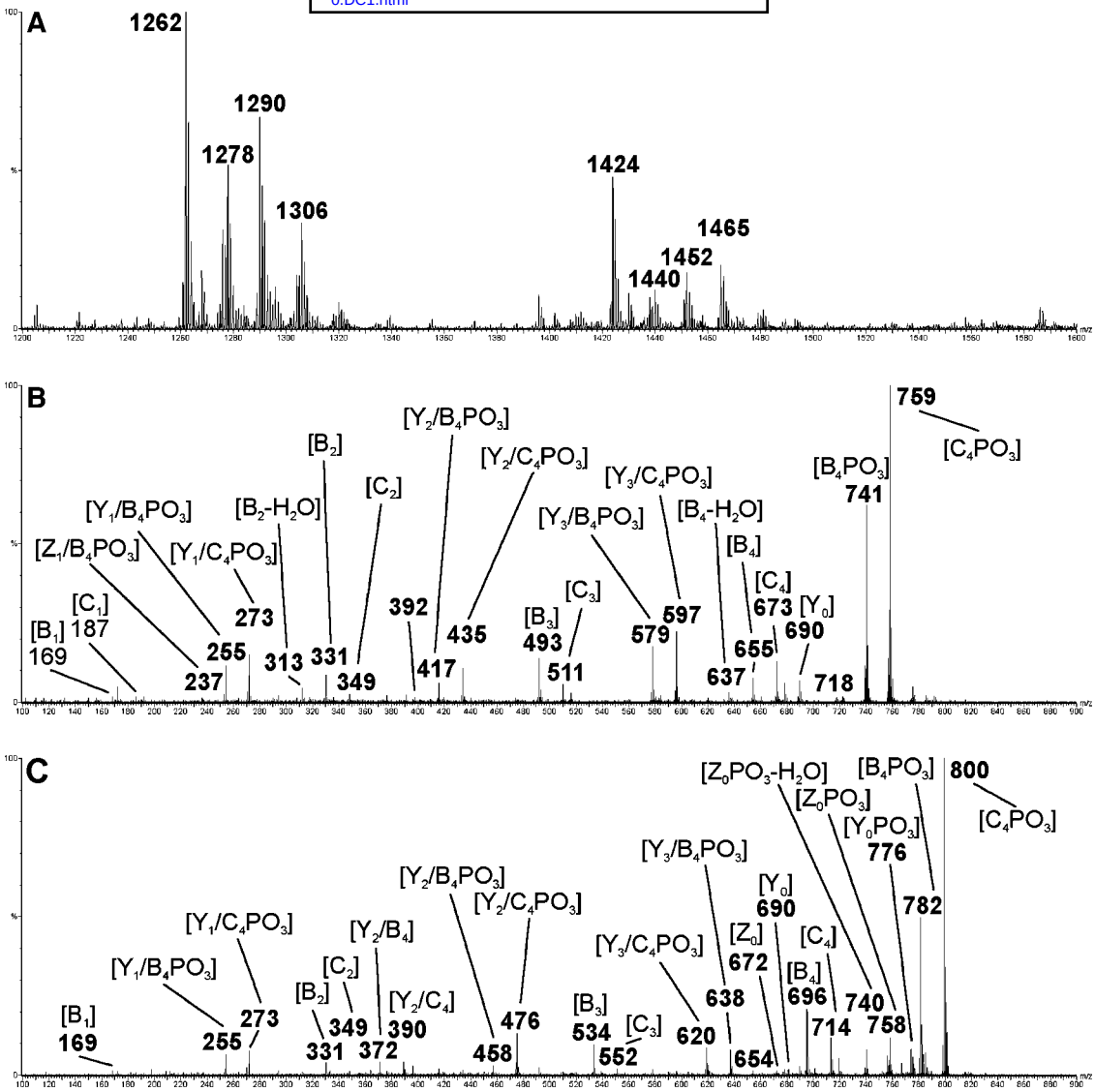

Fig. 13. $^{+}$ESI-Qq/oa-TOF spectra of mixed fraction containing **Af-3c***. A: Profile of molecular ions as $[M(Li)+Li]^{+}$ adducts. B: MS/CID-MS of $[M(Li)+Li]^{+}$ at *m/z* 1,424, low *m/z* region. C: MS/CID-MS of $[M(Li)+Li]^{+}$ at *m/z* 1,465, low *m/z* region. Ion designations for C correspond to Scheme 6; R = NAc. The designations "+Li" and "(Li)+Li" and the charge form have been omitted from the fragment labels for clarity.

the expected structure (data not shown). Similarly, the higher *m/z* $[M(Li)+Li]^{+}$ ions (*m/z* 1,424 and 1,452) are those consistent with the presence of smaller, but significant, amounts of triglycosyl-IPCs, either **Af-3a**, **Af-3b**, or both. This assessment was confirmed by $^{+}$ESI-MS/CID-MS with sequential selection of each of these ions (Fig. 13B; only the result from *m/z* 1,424 is shown). In this profile, an additional ion resulting from underlithiation is clearly observable at *m/z* 1,440; strikingly, however, the underlithiated "satellite" for *m/z* 1,452, expected at *m/z* 1,468, is strongly overlapped by a disproportionately more abundant ion at *m/z* 1,465. Moreover, the odd *m/z* of the ion suggested the presence of another N atom in the structure (as prescribed by the "nitrogen rule"), such as would be contributed by an amino sugar. This was confirmed by $^{+}$ESI-MS/CID-MS of the ion. As shown in Fig. 13C, the resulting product ion spectrum is essentially identical to that obtained previously for the artificially *N*-acetylated **Af-3c** (Fig. 13B), suggesting the presence in *A. fumigatus* GIPCs of a small amount of incompletely de-*N*-acetylated GlcNAcα2IPC precursor (**Af-3c***), apparently also processed by the subsequent mannosylation steps.

This was confirmed by an appraisal of the ^{1}H-NMR spectrum of this fraction (data not shown), which showed the expected preponderance of **Af-2**, as indicated by the pair of α-Man*p* H-1 resonances at 5.057 and 4.894 ppm. The spectrum also exhibited a number of lower intensity resonances that appeared to correlate with those expected for triglycosyl-IPCs **Af-3a** (5.026 ppm) and **Af-3b** (4.993 and 4.829 ppm), but in addition a minor resonance was observed at 4.631 ppm, which is near to that for Manα6 H-1 of **Af-3c**. Subsequently, a spectrum of chemically *N*-acetylated fraction **Af-3c** was acquired; this still contained some residual unacetylated material, which facilitated the detection and measurement of small chemical shift differences attributable to the derivatization (data not shown).

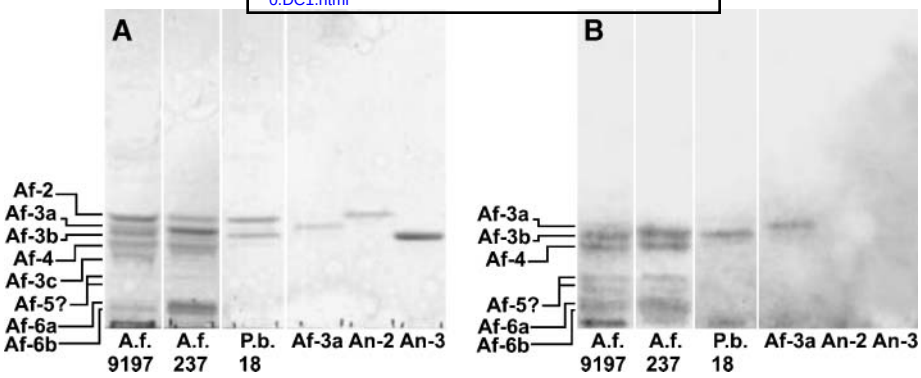

Fig. 14. HPTLC immunostaining of crude and purified fungal GIPC fractions by serum from a patient with disseminated aspergillosis. A: Orcinol staining. B: Serum immunostaining. Crude acidic fractions are as follows: lane 1, *A. fumigatus* (A.f.) strain 9197; lane 2, *A. fumigatus* strain 237; lane 3, *P. brasiliensis* (P.b.) strain 18. Purified GIPC fractions are as follows: lane 4, **Af-3a** from *A. fumigatus* strain 237; lane 5, **An-3** from *A. nidulans* strain A28; lane 6, **An-5** from *A. nidulans* strain A28.

The spectrum showed a measurable downfield shift change of the Manα6 H-1 upon *N*-acetylation of the GlcN residue, from 4.621 to 4.632 ppm, whereas the GlcNα2 H-1 is shifted upfield in this spectrum by ~−0.03 ppm. The chemical shift of the Manα3 H-1 is essentially unchanged by the *N*-acetylation. The observed minor resonance at 4.631 in the spectrum of the mixed fraction is thus also consistent with the presence of *N*-acetylated **Af-3c** (the other expected resonances being partially overlapped with the signals at 4.993 and 4.895 ppm from other components).

Immunoreactivity of *A. fumigatus* GIPCs with aspergillosis serum

In **Fig. 14** are reproduced HPTLC profiles of crude and purified fungal GIPCs stained with orcinol (panel A) and the serum of a patient with aspergillosis (panel B). These compare the reactivity profiles of GIPCs from *A. fumigatus* strains 9197 and 237 (cultured at 37°C; lanes 1 and 2, respectively) with those from *P. brasiliensis* strain 18 (lane 3) as well as the reactivity with purified *A. fumigatus* **Af-3a** (lane 4) and *A. nidulans* components **An-2** and **An-3** (lanes 5 and 6, respectively). These show more extensive staining, including most of the significant bands from both *A. fumigatus* strains (Fig. 14B, lanes 1 and 2) and *P. brasiliensis* **Pb-3** (Fig. 14B, lane 3) and the purified **Af-3a** (Fig. 14B, lane 4). The latter staining shows unambiguously in this case that **Af-3a** is reactive with the serum, along with components **Af-3b**/**Pb-3** and **Af-4**. A variety of lower R_f components from *A. fumigatus* also reacted with the serum. The M_2IPC and M_3IPC components (**An-2** and **An-3**, respectively) from the nonpathogenic *A. nidulans* appeared to be nonreactive (Fig. 14B, lanes 5, 6).

DISCUSSION

The results presented here show that *A. fumigatus* synthesizes, in addition to InsPCer, a complex mixture of GIPCs containing ~10–12 components apparent on HPTLC analysis. In this work, five of the most abundant and least complex of these components were characterized: **Af-2**, Man*p*α3Man*p*α2InsPCer; **Af-3a**, Man*p*α2Man*p*α3Man*p*α2-InsPCer; **Af-3b**, Man*p*α3(Gal*f*β6)Man*p*α2InsPCer; **Af-4**, Man*p*α2Man*p*α3(Gal*f*β6)Man*p*α2InsPCer; and **Af-3c**, Man*p*α3Man*p*α6GlcN*p*α2InsPCer. In addition, the likely biosynthetic precursor to **Af-3c**, in which the GlcN residue is *N*-acetylated, was detected as a minor component in a mixture of triglycosyl-IPCs (referred to as **Af-3c*** and discussed further below). Of these GIPCs, **Af-3a**, **Af-3c***, and **Af-4** have structures that were unreported previously.

Af-2 represents an apparently common intermediate dimannosyl-IPC that has now been found in a number of mycelial or dimorphic euascomycete fungi (**Scheme 7**, **Eu-2a**) (20–22, 30, 39, 40)[4] but has not been reported in hemiascomycetous yeasts such as *S. cerevisiae* and *Candida albicans* (54), nor in any basidiomycete species (52, 55, 56), with the sole exception of *Cantharellus cibarius* (chantarelle) (52). In *S. cerevisiae* and *C. albicans*, GIPC biosynthesis diverges (Scheme 7, IPMα2IPC) by addition of a second mole of *myo*-inositol-1-phosphate to the Man residue of mannosyl-IPC, a process shown in *S. cerevisiae* to be dependent on the *IPT1* gene (57). In basidiomycetes, on the other hand, the dominant structural modification of mannosyl-IPC appears to be conversion to the alternative intermediate diglycosyl-IPC Gal*p*(β1→6)Man*p*(α1→2)InsPCer (Scheme 7, **Ba-2**), which precedes further glycosylation steps in the formation of diverse "basidiolipids" which are found in mushrooms (52, 55), as well as in GIPCs of the yeast-like basidiomycete mycopathogen *Cr. neoformans* (56). The Gal*p*β6- and Man*p*α3-transferases responsible for the further glycosylation of Man*p*(α1→2)InsPCer in euascomycetes and basidiomycetes, respec-

[4] Although Barr, Laine, and Lester (21) did not specify precisely the linkage between Man and Ins in their compounds, but characterized it as Manα1→2/6Ins, NMR spectroscopy of *H. capsulatum* GIPCs (S. B. Levery, M. S. Toledo, A. H. Straus, and H. K. Takahashi, unpublished data) shows that the linkage is Manα1→2Ins1-P-1Cer, as reported previously for GIPCs of *P. brasiliensis* (30) and many other fungi (40, 52, 56).

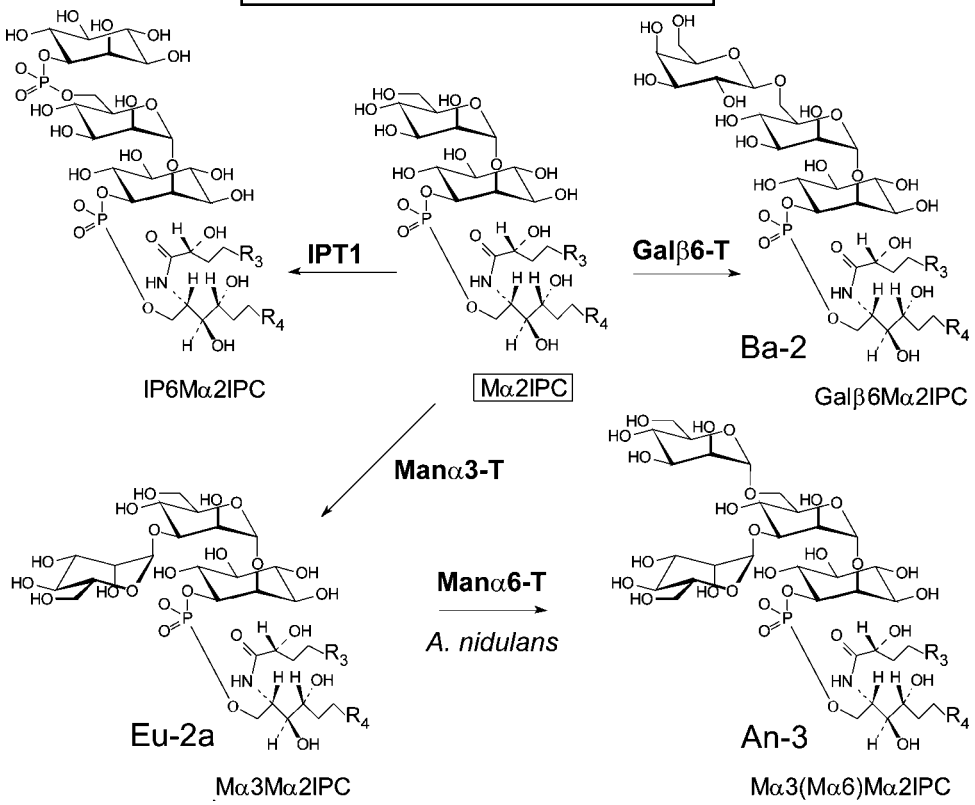

Scheme 7. Divergent structures and hypothetical pathways for the biosynthesis of GIPCs from the common mannosyl-IPC intermediate Manα1→2InsPCer (Mα2IPC). These include InsP1→6Manα1→2InsPCer, a known product of the *IPT1*-encoded enzyme that transfers a second mole of *myo*-inositol-1-*O*-phosphate from phosphatidylinositol to Mα2IPC (left arrow) in *S. cerevisiae*. In basidiomycetes, a commonly observed inter mediate GIPC is Galβ1→6Manα1→2InsPCer (Galβ6Mα2IPC; **Ba-2**), synthesized from Mα2IPC by an as yet unknown Galβ6-T (right arrow). In euascomycetes, a commonly observed intermediate GIPC is Manα1→3Manα1→2InsPCer (Manα3Mα2IPC; **Eu-2a**), synthesized from Mα2IPC by an as yet unknown Manα3-T (lower left). In *A. nidulans*, the major GIPC is a nonantigenic trimannosyl-IPC, Manα1→3(Manα1→6)Manα1→2InsPCer (Manα3[Manα6]Mα2IPC; **An-3**), derived from **Eu-2a** by the addition of a Manα1→6 residue.

tively, remain unidentified. In *A. nidulans*, the major GIPC was found to be the product of **An-2** (= **Eu-2a**) with a Manα6-transferase to yield a branched tri-α-mannosyl structure (Scheme 7, **An-3**) similar to that of the $Man_3GlcNAc_2$ core of protein N-linked glycans (except in that case the branching Man residue is β-, rather than α-).

Among the triglycosyl-IPCs found in *A. fumigatus*, **Af-3b** has been reported previously as a component of both yeast and mycelial forms of the dimorphic mycopathogen *P. brasiliensis* (30). A closely related structural variant, identical to **Af-3b** but possessing a branching α-, rather than β-, Gal*f* residue was reported among the GIPCs of the dimorphic mycopathogen *Histoplasma capsulatum* (20, 21).[4] The *H. capsulatum* antigen was strongly reactive with sera from patients with histoplasmosis, but, unlike the case with *P. brasiliensis*, it was detected only in GIPCs from the yeast form. The glycosylinositol structure of **Af-3a** is novel, apparently unreactive with MEST-1 but reactive with polyclonal sera from a patient with aspergillosis. The tetraglycosyl-IPC **Af-4**, reactive with both MEST-1 and aspergillosis serum, appears to be a product of further glycosylation of the Man*p*α3 unit in **Af-3a** or **Af-3b** by Gal*f*β6 or Man*p*α2 residues, respectively; putative convergent pathways to **Af-4** via these intermediate triglycosyl-IPC structures are illustrated in **Scheme 8**.

The identification of **Af-3c**, which contains a nonacetylated GlcN*p* residue linked α1→2 to Ins, is highly significant in several respects. A GIPC with this structure was originally isolated and characterized from the yeast form of the dimorphic mycopathogen *S. schenckii* (23); at that time, it was pointed out that the GlcN*p*α1→2Ins linkage is isomeric to the GlcN*p*α1→6Ins linkage found in the core of all protein and phosphoglycan glycosylphosphatidylinositol (GPI) anchors (58–60). Since that time, GPI anchors of *A. fumigatus* proteins have been characterized and found to have hexaglycosylinositol phosphorylceramide core structures: Manα3Manα2Manα2Manα6Manα4GlcNα6InsPCer (61). In addition, a 30 kDa galactomannan from *A. fumigatus* was found to be anchored by a GPI with a similar core structure, although in this case the linkage of GlcN to Ins was not defined unambiguously: Manα2Manα2Manα6Manα4GlcN[x]InsPCer (62). It is worth noting that the GlcN-containing GIPCs reported here differ from the structure of GPI anchors not only in the GlcN-Ins

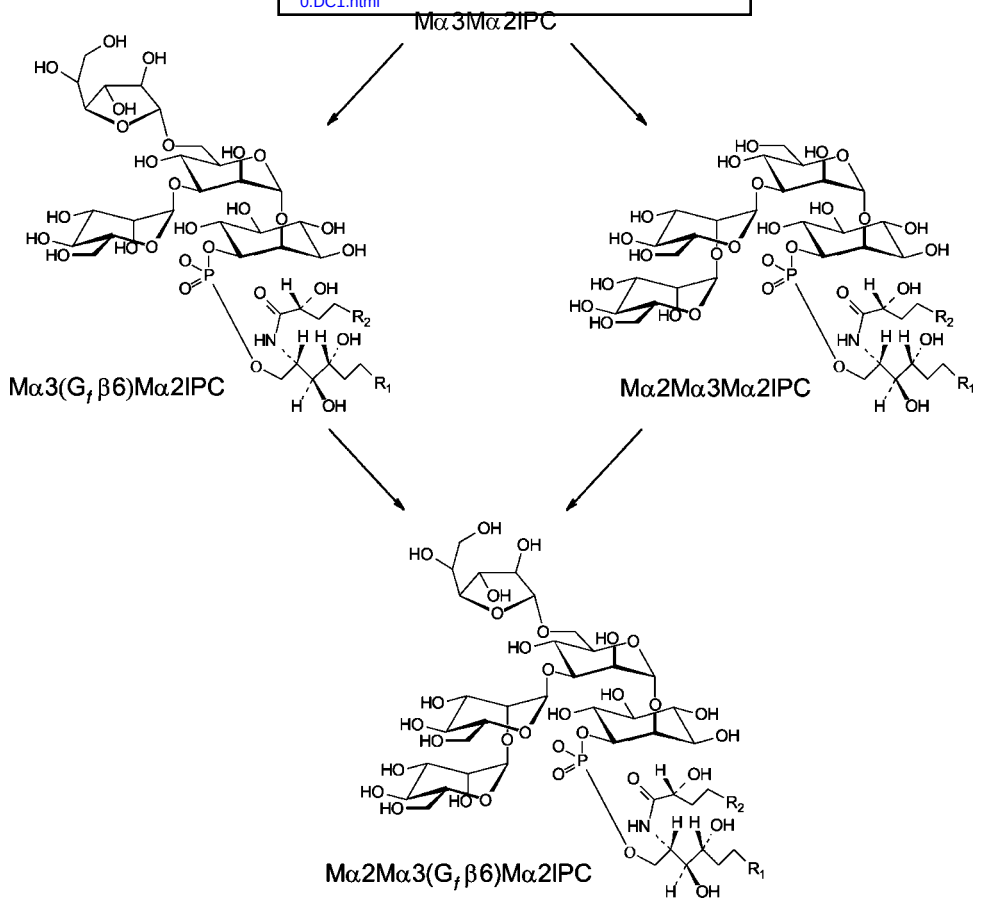

Scheme 8. Structures and hypothetical pathways for the biosynthesis of *A. fumigatus* GIPC antigens **Af-3a**, **Af-3b**, and **Af-4**, starting from the common dimannosyl-IPC intermediate **Af-2**, Manα1→3Manα1→2InsPCer (Manα3Mα2IPC).

linkage position but also in the linkage sequence of the attached Man residues. Thus, they appear to be synthesized by a pathway altogether distinct.

On the other hand, it was hypothesized that, similar to the case with GlcN*p*α1→6Ins of GPI anchors, the GlcN*p*α1→2Ins structure might be formed by a process requiring two enzymes: transfer of GlcNAc to the Ins moiety, followed by de-*N*-acetylation of the GlcNAc residue (23). More recently, a series of novel GIPCs, also based on the GlcN*p*α1→2Ins core structure, was isolated from mycelia of *Acremonium* species (31). In this case, the alternative triglycosyl-IPC structure Man*p*(α1→6)Man*p*(α1→6)GlcN*p*(α1→2)InsPCer was identified, along with all of the presumptive intermediates. In addition, a remarkable finding was the addition of phosphocholine to the 6-hydroxyl of the terminal α-Man*p* residues of both Man*p*(α1→6)GlcN*p*(α1→2)InsPCer and Man*p*(α1→6)Man*p*(α1→6)GlcN*p*(α1→2)InsPCer. The suggestion of a two-step conversion of InsPCer to the core intermediate GlcN*p*(α1→2)InsPCer was again invoked (31). We propose that the small amount of triglycosyl-IPC observed in a mixed fraction of *A. fumigatus* GIPCs (**Af-3c***), clearly containing a HexNAc residue directly linked to Ins, is Man*p*(α1→3)Man*p*(α1→6)GlcNAc*p*(α1→2)InsPCer: in other words, a structural analog of **Af-3c** derived from incompletely de-*N*-acetylated GlcNAc*p*(α1→2)InsPCer. Although this needs further confirmation, it lends support to the suggestion that a two-step process, similar to that observed for GlcN*p*α1→6Ins in the GPI anchor pathway, also applies to GlcN*p*α1→2Ins in the GIPC pathway. Whether the same de-*N*-acetylase could be involved is an interesting question that should be answered by further in vitro and in vivo studies. A more important question, of course, is whether any special functional role(s) might be associated with this zwitterionic class of GIPCs, with or without the addition of phosphocholine. In this regard, it is significant that the *Acremonium* species GIPCs were found to induce cell death in suspension-cultured rice cells (31).

Thus, we consider that three core motifs have been confirmed at the monosaccharide level for fungal GIPCs (by identification in structural studies from at least two different laboratories); these are Manα1→2Ins, Manα1→6Ins, and GlcNα1→2Ins (Scheme 1). Of these, the Manα1→6Ins core has been reported only for GIPCs of *S. schenckii* (22, 24); remarkably, *S. schenckii* expresses GIPCs with all three core structures (23). As shown in the current study, *A. fumigatus* is sufficiently versatile at least to use two of these. Notably, the GlcNα1→2Ins core has not been observed in GIPCs from the related model fungus *A. nidulans*; to date, only oligo-α-mannosyl-IPCs, based on

the Man*p*(α1→3)Man*p*(α1→2)InsPCer core, have been isolated from *A. nidulans*, with no evidence for the expression of antigenic determinants containing β-Gal*f* residues (40). This interesting dichotomy suggests that wider versatility in GIPC biosynthesis may be one factor in the survival of *A. fumigatus* in highly diverse environments, including the entire range of mammalian host cells, tissues, and organs.

The authors thank James Rankin and Emma Arigi for technical assistance with growing *A. fumigatus* cultures and isolating some of the title compounds. This work was supported by Fundação de Amparo à Pesquisa do Estado de São Paolo and Conselho Nacional de Desenvolvimento Científico e Technológico (Brasil) (M.S.T., A.H.S., and H.K.T.), a Glycoscience Research Award from Neose Technologies, Inc., the National Institutes of Health Resource Center for Biomedical Complex Carbohydrates (Grant P41 RR-05351), and the Biological Research Infrastructure Network-Center for Structural Biology (Grant P20 RR-16459).

REFERENCES

1. Rüchel, R., and U. Reichard. 1999. Pathogenesis and clinical presentation of aspergillosis. *In Aspergillus fumigatus*: Biology, Clinical Aspects and Molecular Approaches to Pathogenicity. A. A. Brakhage, B. Jahn, and A. Schmidt, editors. Karger, Basel, Switzerland. 21–43.
2. Latge, J. P. 2001. The pathobiology of *Aspergillus fumigatus*. *Trends Microbiol.* **9:** 382–389.
3. Brakhage, A. A., and K. Langfelder. 2002. Menacing mold: the molecular biology of *Aspergillus fumigatus*. *Annu. Rev. Microbiol.* **56:** 433–455.
4. Schmitt, H. J., A. Blevins, K. Sobeck, and D. Armstrong. 1990. Aspergillus species from hospital air and from patients. *Mycoses.* **33:** 539–541.
5. Schaffner, A. 1985. Therapeutic concentrations of glucocorticoids suppress the antimicrobial activity of human macrophages without impairing their responsiveness to gamma interferon. *J. Clin. Invest.* **76:** 1755–1764.
6. Verweij, P. E., and D. W. Denning. 1997. Diagnostic and therapeutic strategies for invasive aspergillosis. *Semin. Respir. Crit. Care Med.* **18:** 203–215.
7. Bolard, J. 1986. How do the polyene macrolide antibiotics affect the cellular membrane properties? *Biochim. Biophys. Acta.* **864:** 257–304.
8. Moore, C. B., N. Sayers, J. Mosquera, J. Slaven, and D. W. Denning. 2000. Antifungal drug resistance in Aspergillus. *J. Infect.* **41:** 203–220.
9. Georgopapadakou, N. H. 2000. Antifungals targeted to sphingolipid synthesis: focus on inositol phosphorylceramide synthase. *Expert Opin. Investig. Drugs.* **9:** 1787–1796.
10. Nagiec, M. M., E. E. Nagiec, J. A. Baltisberger, G. B. Wells, R. L. Lester, and R. C. Dickson. 1997. Sphingolipid synthesis as a target for antifungal drugs. Complementation of the inositol phosphorylceramide synthase defect in a mutant strain of *Saccharomyces cerevisiae* by the *AUR1* gene. *J. Biol. Chem.* **272:** 9809–9817.
11. Takesako, K., H. Kuroda, T. Inoue, F. Haruna, Y. Yoshikawa, and I. Kato. 1993. Biological properties of aureobasidin A, a cyclic depsipeptide antifungal antibiotic. *J. Antibiot.* **49:** 1414–1420.
12. Mandala, S. M., R. A. Thornton, M. Rosenbach, J. Milligan, M. Garcia-Calvo, H. G. Bull, and M. B. Kurtz. 1997. Khafrefungin, a novel inhibitor of sphingolipid synthesis. *J. Biol. Chem.* **272:** 32709–32714.
13. Mandala, S. M., R. A. Thornton, J. Milligan, M. Rosenbach, M. Garcia-Calvo, H. G. Bull, G. Harris, G. K. Abruzzo, A. M. Flattery, C. J. Gill, et al. 1998. Rustmicin, a potent antifungal agent, inhibits sphingolipid synthesis at the inositol phosphoceramide synthase. *J. Biol. Chem.* **273:** 14942–14949.
14. Hashida-Okado, T., R. Yasumoto, M. Endo, K. Takesako, and I. Kato. 1998. Isolation and characterization of the aureobasidin A-resistant gene, aur1R, on *Schizosaccharomyces pombe*: roles of Aur1p+ in cell morphogenesis. *Curr. Genet.* **33:** 38–45.
15. Kuroda, M., T. Hashida-Okado, R. Yasumoto, K. Gomi, I. Kato, and K. Takesako. 1999. An aureobasidin A resistance gene isolated from Aspergillus is a homolog of yeast AUR1, a gene responsible for inositol phosphorylceramide (IPC) synthase activity. *Mol. Gen. Genet.* **261:** 290–296.
16. Heidler, S. A., and J. A. Radding. 1995. The *AUR1* gene in *Saccharomyces cerevisiae* encodes a dominant resistance to the antifungal agent aureobasidin A (LY295337). *Antimicrob. Agents Chemother.* **39:** 2765–2769.
17. Heidler, S. A., and J. A. Radding. 2000. Inositol phosphoryl transferases from human pathogenic fungi. *Biochim. Biophys. Acta.* **1500:** 147–152.
18. Hashida-Okado, T., A. Ogawa, M. Endo, R. Yasumoto, K. Takesako, and I. Kato. 1996. *AUR1*, a novel gene conferring aureobasidin resistance on *Saccharomyces cerevisiae*: a study of defective morphologies in Aur1p-depleted cells. *Mol. Gen. Genet.* **251:** 236–244.
19. Dickson, R. C., and R. L. Lester. 2002. Sphingolipid functions in *Saccharomyces cerevisiae*. *Biochim. Biophys. Acta.* **1583:** 13–25.
20. Barr, K., and R. L. Lester. 1984. Occurrence of novel antigenic phosphoinositol-containing sphingolipids in the pathogenic yeast *Histoplasma capsulatum*. *Biochemistry.* **23:** 5581–5588.
21. Barr, K., R. A. Laine, and R. L. Lester. 1984. Carbohydrate structures of three novel phosphoinositol-containing sphingolipids from the yeast *Histoplasma capsulatum*. *Biochemistry.* **23:** 5589–5596.
22. Toledo, M. S., S. B. Levery, J. Glushka, A. H. Straus, and H. K. Takahashi. 2001. Structure elucidation of sphingolipids from the mycopathogen *Sporothrix schenckii*: identification of novel glycosylinositol phosphorylceramides with core Manα1→6Ins linkage. *Biochem. Biophys. Res. Commun.* **280:** 19–24.
23. Toledo, M. S., S. B. Levery, A. H. Straus, and H. K. Takahashi. 2001. Sphingolipids of the mycopathogen *Sporothrix schenckii*: identification of a glycosylinositol phosphorylceramide novel core GlcNH2α1→2Ins motif. *FEBS Lett.* **493:** 50–56.
24. Loureiro y Penha, C. V., A. R. Todeschini, L. M. Lopes-Bezerra, R. Wait, C. Jones, K. A. Mattos, N. Heise, L. Mendonca-Previato, and J. O. Previato. 2001. Characterization of novel structures of mannosylinositolphosphorylceramides from the yeast forms of *Sporothrix schenckii*. *Eur. J. Biochem.* **268:** 4243–4250.
25. Suzuki, E., M. S. Toledo, H. K. Takahashi, and A. H. Straus. 1997. A monoclonal antibody directed to terminal residue of β-galactofuranose of a glycolipid antigen isolated from *Paracoccidioides brasiliensis*: cross-reactivity with *Leishmania major* and *Trypanosoma cruzi*. *Glycobiology.* **7:** 463–468.
26. Straus, A. H., E. Suzuki, M. S. Toledo, C. M. Takizawa, and H. K. Takahashi. 1995. Immunochemical characterization of carbohydrate antigens from fungi, protozoa and mammals by monoclonal antibodies directed to glycan epitopes. *Braz. J. Med. Biol. Res.* **28:** 919–923.
27. Toledo, M. S., E. Suzuki, A. H. Straus, and H. K. Takahashi. 1995. Glycolipids from *Paracoccidioides brasiliensis*. Isolation of a galactofuranose-containing glycolipid reactive with sera of patients with paracoccidioidomycosis. *J. Med. Vet. Mycol.* **33:** 247–251.
28. Jennemann, R., B. L. Bauer, H. Bertalanffy, T. Selmer, and H. Wiegandt. 1999. Basidiolipids from *Agaricus* are novel immune adjuvants. *Immunobiology.* **200:** 277–289.
29. Jennemann, R., R. Sandhoff, H-J. Grone, and H. Wiegandt. 2001. Human heterophile antibodies recognizing distinct carbohydrate epitopes on basidiolipids from different mushrooms. *Immunol. Invest.* **30:** 115–129.
30. Levery, S. B., M. S. Toledo, A. H. Straus, and H. K. Takahashi. 1998. Structure elucidation of sphingolipids from the mycopathogen *Paracoccidioides brasiliensis*: an immunodominant β-galactofuranose residue is carried by a novel glycosylinositol phosphorylceramide antigen. *Biochemistry.* **37:** 8764–8775.
31. Aoki, K., R. Uchiyama, S. Itonori, S. Sugita, F-S. Che, A. Isogai, N. Hada, T. Takeda, H. Kumagai, and K. Yamamoto. 2004. Structural elucidation of novel phosphocholine-containing glycosylinositolphosphoceramide in filamentous fungi and their induction of cell death of cultured rice cells. *Biochem. J.* **378:** 461–472.
32. Kafer, E. 1977. Meiotic and mitotic recombinations in *Aspergillus* and its chromosomal aberrations. *Adv. Genet.* **19:** 33–131.
33. Magnani, J. L., D. F. Smith, and V. Ginsburg. 1980. Detection of gangliosides that bind toxin: direct binding of ^{125}I-labeled toxin to thin-layer chromatography. *Anal. Biochem.* **109:** 399–402.
34. Kannagi, R., E. Nudelman, S. B. Levery, and S. Hakomori. 1982. A series of human erythrocyte glycosphingolipids reacting to the

monoclonal antibody directed to a developmentally regulated antigen, SSEA-1. *J. Biol. Chem.* **257:** 14865–14874.
35. Suzuki, E., A. K. Tanaka, M. S. Toledo, H. K. Takahashi, and A. H. Straus. 2002. Role of beta-D-galactofuranose in *Leishmania major* macrophage invasion. *Infect. Immun.* **70:** 6592–6596.
36. Levery, S. B., M. Momany, R. Lindsey, M. S. Toledo, J. A. Shayman, M. Fuller, K. Brooks, R. L. Doong, A. H. Straus, and H. K. Takahashi. 2002. Disruption of the glucosylceramide biosynthesis pathway in *Aspergillus nidulans* and *Aspergillus fumigatus* by inhibitors of UDP-Glc: ceramide glucosyltransferase strongly affects spore germination, cell cycle, and hyphal growth. *FEBS Lett.* **525:** 59–64.
37. Toledo, M. S., S. B. Levery, A. H. Straus, E. Suzuki, M. Momany, J. Glushka, J. M. Moulton, and H. K. Takahashi. 1999. Characterization of sphingolipids from mycopathogens: factors correlating with expression of 2-hydroxy fatty acyl (*E*)-Δ^3-unsaturation in cerebrosides of *Paracoccidioides brasiliensis* and *Aspergillus fumigatus*. *Biochemistry.* **38:** 7294–7306.
38. Dabrowski, J., P. Hanfland, and H. Egge. 1980. Structural analysis of glycosphingolipids by high-resolution ^{1}H nuclear magnetic resonance spectroscopy. *Biochemistry.* **19:** 5652–5658.
39. Levery, S. B., M. S. Toledo, A. H. Straus, and H. K. Takahashi. 2001. Comparative analysis of glycosylinositol phosphorylceramides from fungi by electrospray tandem mass spectrometry with low-energy collision-induced dissociation of Li^+ adduct ions. *Rapid Commun. Mass Spectrom.* **15:** 2240–2258.
40. Bennion, B., C. Park, M. Fuller, R. Lindsey, M. Momany, R. Jennemann, and S. B. Levery. 2003. Glycosphingolipids of the model fungus *Aspergillus nidulans*: characterization of GIPCs with oligo-α-mannose-type glycans. *J. Lipid Res.* **44:** 2073–2088.
41. Levery, S. B. 2005. Glycosphingolipid structural analysis and glycosphingolipidomics. *Methods Enzymol.* **405:** 300–369.
42. Adams, J., and Q. Ann. 1993. Structure determination of sphingolipids by mass spectrometry. *Mass Spectrom. Rev.* **12:** 51–85.
43. Singh, B. N., C. E. Costello, and D. H. Beach. 1991. Structures of glycophosphosphingolipids of *Tritrichomonas foetus*: a novel glycophosphosphingolipid. *Arch. Biochem. Biophys.* **286:** 409–418.
44. Hsu, F. F., and J. Turk. 2001. Structural determination of glycosphingolipids as lithiated adducts by electrospray ionization mass spectrometry using low-energy collisional-activated dissociation on a triple stage quadrupole instrument. *J. Am. Soc. Mass Spectrom.* **12:** 61–79.
45. Ciucanu, I., and F. Kerek. 1984. A simple and rapid method for the permethylation of carbohydrates. *Carbohydr. Res.* **131:** 209–217.
46. Levery, S. B., and S. Hakomori. 1987. Microscale methylation analysis of glycolipids using capillary gas chromatography-chemical ionization mass fragmentography with selected ion monitoring. *Methods Enzymol.* **138:** 13–25.
47. Laine, R. A., N. D. Young, J. N. Gerber, and C. C. Sweeley. 1974. Identification of 2-hydroxy fatty acids in complex mixtures of fatty acid methyl esters by mass chromatography. *Biomed. Mass Spectrom.* **1:** 10–14.
48. Thorpe, S. R., and C. C. Sweeley. 1967. Chemistry and metabolism of sphingolipids. On the biosynthesis of phytosphingosine by yeast. *Biochemistry.* **6:** 887–897.
49. Gaver, R. C., and C. C. Sweeley. 1966. Chemistry and metabolism of sphingolipids. 3-Oxo derivatives of *N*-acetylsphingosine and *N*-acetyldihydrosphingosine. *Biochemistry.* **88:** 3643–3647.
50. Polito, A. J., T. Akita, and C. C. Sweeley. 1968. Gas chromatography and mass spectrometry of sphingolipid bases. Characterization of sphinga-4,14-dienine from plasma sphingomyelin. *Biochemistry.* **7:** 2609–2614.
51. Brisson, J-R., and J. P. Carver. 1983. Solution conformation of asparagine-linked oligosaccharides: α(1-2)-, α(1-3)-, β(1-2)-, and β(1-4)-linked units. *Biochemistry.* **22:** 3671–3680.
52. Jennemann, R., R. Geyer, R. Sandhoff, R. M. Gschwind, S. B. Levery, H-J. Gröne, and H. Wiegandt. 2001. Glycoinositolphosphosphingolipids (basidiolipids) of higher mushrooms. *Eur. J. Biochem.* **268:** 1190–1205.
53. Gorin, P. A. J. 1981. Carbon-13 nuclear magnetic resonance spectroscopy of polysaccharides. *Adv. Carbohydr. Chem. Biochem.* **38:** 13–104.
54. Dickson, R. C., and R. L. Lester. 1999. Yeast sphingolipids. *Biochim. Biophys. Acta.* **1426:** 347–357.
55. Jennemann, R., B. L. Bauer, H. Bertalnffy, R. Geyer, R. M. Gschwind, T. Selmer, and H. Wiegandt. 1999. Novel glycoinositolphosphosphingolipids, basidiolipids, from *Agaricus*. *Eur. J. Biochem.* **259:** 331–338.
56. Heise, N., A. L. S. Gutierrez, K. A. Mattos, C. Jones, R. Wait, J. O. Previato, and L. Mendonca-Previato. 2002. Molecular analysis of a novel family of complex glycoinositolphosphoryl ceramides from *Cryptococcus neoformans*: structural differences between encapsulated and acapsular yeast forms. *Glycobiology.* **12:** 409–420.
57. Dickson, R. C., E. E. Nagiec, G. B. Wells, M. M. Nagiec, and R. L. Lester. 1997. Synthesis of mannose-(inositol-P)$_2$-ceramide, the major sphingolipid in *Saccharomyces cerevisiae*, requires the *IPT1* (*YDR072c*) gene. *J. Biol. Chem.* **272:** 29620–29625.
58. Ferguson, M. A. J., and A. F. Williams. 1988. Cell-surface anchoring of proteins via glycosyl-phosphatidylinositol structures. *Annu. Rev. Biochem.* **57:** 285–320.
59. Englund, P. T. 1993. The structure and biosynthesis of glycosyl phosphatidylinositol protein anchors. *Annu. Rev. Biochem.* **62:** 121–138.
60. de Lederkremer, R. M., and W. Colli. 1995. Galactofuranose-containing glycoconjugates in trypanosomatids. *Glycobiology.* **5:** 547–552.
61. Fontaine, T., T. Magnin, A. Melhert, D. Lamont, J. P. Latge, and M. A. Ferguson. 2003. Structures of the glycosylphosphatidylinositol membrane anchors from *Aspergillus fumigatus* membrane proteins. *Glycobiology.* **13:** 169–177.
62. Costachel, C., B. Coddeville, J. P. Latge, and T. Fontaine. 2005. Glycosylphosphatidylinositol-anchored fungal polysaccharide in *Aspergillus fumigatus*. *J. Biol. Chem.* **280:** 39835–39842.